Cement & Concrete Composites 31 (2009) 39–59

Contents lists available at ScienceDirect

Cement & Concrete Composites

journal homepage: www.elsevier.com/locate/cemconcomp

Flow analysis of water–powder mixtures: Application to specific surface area and shape factor

M. Hunger *, H.J.H. Brouwers

Department of Civil Engineering, Faculty of Engineering Technology, University of Twente, P.O. Box 217, 7500 AE Enschede, The Netherlands

ARTICLE INFO

Article history:
Received 4 February 2008
Received in revised form 18 September 2008
Accepted 26 September 2008
Available online 7 October 2008

Keywords:
Powder analysis
Water demand
Void fraction
Specific surface area
Spread-flow test
Particle shape factor

ABSTRACT

This paper addresses the characterization of powder materials with respect to their application in concrete. Given that powders provide by far highest percentage of specific surface area in a concrete mix, their packing behavior and water demand is of vital interest for the design of concrete. They dominate physical properties like workability or strength and durability in hardened state.

Regarding the granular properties of powders, different states of packing are analyzed and compared. In reference to water demands, this paper compares and analyzes four different methods, including the spread-flow test. It is shown that linear relations can be derived in order to correlate the methods. Besides comments and modifications to individual tests, the spread-flow test is analyzed in more detail. In this way new measures are derived which contribute to a deeper understanding of wet granular mixtures at the onset of flowing.

Furthermore, the deformation coefficient which is derived by the spread-flow test is confirmed to correlate with the product of Blaine surface and intrinsic density of the individual powders when the mixture is flowing only under its own weight. Similarly, correlations with equal accuracy are found with a computed specific surface, based on measured particle size distributions. Using the flow experiments it is possible to derive an overall factor for assessing the non-spherical shape of the powder particles. It is shown that the computed surface area and the Blaine value have a constant ratio (of about 1.7).

Finally, the value of a constant water layer thickness around the powder particles is computed for all powders at the onset of flowing. This implies the possibility to predict flow behavior of paste only based on the knowledge of their specific surface area, either determined by computation or Blaine measurements.

1. Introduction

Powder analysis is considered to be an important part of industry and research. The knowledge of powder properties is necessary to control product attributes and the way of processing powders. This holds for all sectors of industry such as the paint, ceramic or rubber industry. In many cases emphasis is put on the packing of different powders within each other or in coarser granular fractions. This also holds for concrete industry. Because of the nature of concrete, here emphasis is placed on wet powders [1].

The macroscopic properties of concrete such as strength or durability are guided by the properties of the matrix, the aggregates, and the bond behavior of matrix and aggregates. Cement, mixing water, air, the fines content of the aggregate, and possibly admixtures and additions are considered to form the matrix. In other words, the matrix is composed of water, air and powder [2]. The latter is in concrete technology usually defined as any particle being smaller than 125 μm. This boundary value appears to be a suitable measure, at least for the metric unit system. Though it is less appropriate for the interests of powder technology which usually is using smaller particles sizes, it is rather important for concrete industry as the majority of cements are included in this size range and standard sieve lines stop at this size.

The characteristic of the matrix and the bond behavior between aggregate and matrix are dependent on a number of factors, of which the effective water/cement ratio (or water/powder ratio), and the reactivity, particle shape and particle size distribution of the powders are the most important ones. Furthermore, for a dense grain packing in the matrix not only an optimized granular build-up of the solids is necessary [1] but also the water content will influence the state of packing [3]. This concept has been successfully applied by Hunger and Brouwers [4] for the production of self-compacting concretes (SCC). During a stepwise saturation of a granular mixture, first all voids are filled with water. This process is accompanied by the generation of water films around the particles. Having a filled void fraction, i.e. saturated or supersaturated conditions, the present ratio of total specific surface area to the remaining

* Corresponding author.
E-mail address: m.hunger@ctw.utwente.nl (M. Hunger).

0958-9465/$ - see front matter © 2008 Elsevier Ltd. All rights reserved.
doi:10.1016/j.cemconcomp.2008.09.010

Nomenclature

BET	Brunauer–Emmet–Teller method
GCC	ground calcium carbonate
OPC	ordinary Portland cement
RCP	random close packing
RLP	random loose packing
sc	simple cubic
SCC	self-compacting concrete
SSA	specific surface area

Romans

A	surface area (m^2)
a	specific surface area, mass-based (m^2/kg)
a_{Blaine}	specific surface area according to the Blaine method (cm^2/g)
E_p	deformation coefficient (–)
d	diameter (m)
P	packing (–)
S	specific surface area, volume based (m^2/m^3)
u	diameter ratio of subsequent fractions (–)
V	volume (m^3)

Greeks

β_p	water/powder percentage (vol.%) for $\Gamma_p = 0$
Γ_p	relative slump of powder suspensions
δ	water layer thickness (m)
ξ	shape factor
ρ	density (kg/m^3)
Φ	void fraction
ω	mass fraction

Subscript

agg	aggregate
app	apparent
arith	arithmetic
comp	compacted
geo	geometric
loose	loose
marq	modified Marquardt test
p	powder
s	specific
sph	spherical, based on spheres
spread	spread-flow test
sur	surface
vibr	vibrated
w	water

amount of water determines significantly the workability of a mixture. Based on this assumption, a water layer thickness can be derived, as shown later on. The increasing thickness of water layers determines the location of particles in the system relative to each other. With further rise of the water content, there is an increase in mean interparticle distance. Then, densest possible packing is not given anymore. Furthermore, depending on the specific density of powders, an increasing tendency to segregation is noticed, since the surplus water can no longer be adsorbed at the particle surfaces. On this account, an accurate determination of the water demand is of importance for the success of a mortar or concrete mixture, in particular if it should provide self-compactibility.

In the following Chapter a number of powders are introduced and characterized regarding their density, void fraction in different modes of packing, and particle size distribution. The introduced powders cover the broad range of powders used in concrete technology. These are for example different cements, non-reactive powders such as limestone powder or reactive powders such as fly ash. In addition fine mineral quarry waste such as marble or granite powder is characterized as well. Based on the particle size distribution a calculation algorithm is derived in order to compute the specific surface area of powders. In another chapter these powders are analyzed regarding their water demand using four different tests methods and comparing these results. Based on the data obtained with the spread-flow test a deeper analysis has been carried out which resulted in a number of new hypotheses. These are for example the concept of constant water layer thickness and the derivation of shape factors based on flow experiments. The latter has been verified by SEM analysis in addition.

2. Characterization of powders

In regard to the large specific surface area which is provided by small particles, characterization of powders is essential for the ability to control physical properties, such as workability of self-compacting concrete. Furthermore, strength development and durability of concrete is effected by the type and amount of applied powder. In the following all applied powder materials are introduced.

2.1. Selected powder materials

2.1.1. Cements

Since blast-furnace cements gain importance in the construction sector (e.g. [5]) a multitude of tests for this research has been performed using two types of a CEM III/B 42.5 N (A and B), being a typical representative of blast-furnace cements. The second blast-furnace cement, type B ($d_{median} \approx 6.5$ μm), shows a finer size distribution than type A ($d_{median} \approx 15$ μm). These cements are known, in contrast to ordinary Portland cements (OPC), to show a slower hydration development but to exhibit later, in particular after 28 days, a denser microstructure, which contributes to the durability of concrete made from these cements. Besides a low effective alkali content (LA) and low hydration heat release (LH), the applied cements offer a high sulfate resistance (HS) as well. OPC CEM I 52.5 N was also tested. Since the significance of ultra fine cements is increasingly recognized in recent years, a micro-cement CEM I 52.5 R was included. Ultra fine powders are of interest for the improvement of packing. Due to their high specific surface area they are also supposed to yield key results in respect to water demands and flow behavior of pastes.

A scheme with the composition of the applied cements can be found in Table 1. Furthermore, Table 2 shows the basic cement characterization according to EN 196. These tests were partly done in the own lab, otherwise data from the respective cement producer is given.

2.1.2. Non-reactive rock flour

Limestone powder, one of the standard filler materials in concrete production, was included in the test series. The deployed limestone powder is a ground calcium carbonate (GCC) originating from natural limestone. In Table 3 the used limestone powder is characterized with regard to its chemical composition.

Table 1
Composition of cements (source: CEMENTA AB (Sweden), ENCI (The Netherlands) and READYMIX Hüttenzement GMBH (Germany)).

Material key number	Portland cement clinker (m.%)	Blast furnace slag (m.%)	Na_2O equivalent (m.%)	Chloride content (Cl^-) (m.%)	Minor constituents (m.%)
CEM I 52.5 N	⩾95	–	–	–	0–5
CEM I 52.5 R - micro-cement	⩾95	–	⩽0.6	⩽0.1	0–5
CEM III/B 42.5 N A	24	72	0.6	0.03	4
CEM III/B 42.5 N B	20–34	66–80	–	–	0–5

Table 2
Cement tests according to EN 196 (source: tests on initial set and norm strength cp. Table 1). Results are based on own measurements and partly on product specifications of the respective cement producer.

Material key number	Initial set (min)	Water demand[a] (wt.%)	Specific density (g/cm^3)	Compressive strength (N/mm^2)		
				2 days	7 days	28 days
CEM I 52.5 N	⩾45	38.9	3.064	⩾30.0	–	⩾52.5
CEM I 52.5 R – micro-cement	30	54.9	3.150	–	–	–
CEM III/B 42.5 N A	243	33.3	2.928	13.7	30.0	52.5
CEM III/B 42.5 N B	⩾60	37.9	2.962	⩾10.0	–	⩾42.5

[a] The water demand is determined according to the spread-flow test.

Table 3
Oxide composition of powders (m.%).

Material key number	Limestone powder (m.%)	Granite powder (m.%)	Marble powder A (m.%)	Fly ash A (m.%)
SiO_2	–	59.5	0.60	47–53
AL_2O_3	–	15.8	0.08	26–30
Fe_2O_3	–	3.6	0.07	5.0–15
CaO	–	4.6	30.4	2.4–3.9
$CaCO_3$	97.84	–	4.0	–
$CaCO_3 + MgCO_3$	99.27	–	95.0	–
MgO	–	1.7	21.9	1.9–2.5
SO_3	0.05	–	–	0.2–2.0
K_2O	0.02	4.3	<0.01	3.0–4.6
Na_2O	0.01	3.2	<0.01	0.6–1.1
Cl	<0.01	–	–	0.01

Fine ground limestone powders can exhibit a limited hydraulic reactivity [30]. This predominantly improves the bond to the surrounding microstructure due to the reaction products, formed on the surface of limestone powder particles. The limestone powder itself, however, is not having structure forming properties and is therefore not noteworthy involved into the strength development. On this account limestone powder is considered to be non-reactive.

Besides limestone powders, which are primary materials, special attention is paid to stone waste materials, generated by the natural stone and ornamental stone industry. In this respect two more powder types are introduced: a granite powder and a marble powder. The latter mineralogically also consists to a larger part of calcium carbonate (calcite or dolomite).

In all quarry operations fines are collected during the whole process chain by particle filter devices. Those fines are in a dry state, which eases their application in concrete mixes but their amount is relatively small in comparison to fines produced during the washing process of broken aggregates. Depending on the type of rock and the applied crushing units this can vary notably. Fines are removed from the material by wet sieving and/or separation in hydrocyclones. The outcome of this process is slurry, highly loaded with a fine fraction. This slurry is sometimes pumped directly into settling ponds where it represents environmental impacts on water and soil. For a better handling afterwards those slurries often become treated by means of a filter press. In that way the water will be removed from the material to a great extent and can be returned into the washing process. Depending on the applied pressure, the pressing time itself and the grading of the fine fraction, the remaining filter cake contains an amount of water from 18–30%. In this state the material can be transported easier by e.g. wheel loaders or band-conveyors and is easily piled. Further sources of fines are all processing steps in the ornamental stone industry. During drilling, grinding, polishing, and most of all, sawing, large volumes of fines are produced. Calmon [6] specifies for the Brazilian situation, the volume fraction of a marble stone block which results in 30% sawing waste producing slabs of 1–3 cm thickness. Laskaridis [7] gives similar figures for a Greek company. Prevention of landfill and a useful application of these rock powders would therefore constitute a great environmental benefit.

The introduced granite powder is accumulated during the washing of aggregates from a granite quarry in Glensanda, Scotland. Subsequent to the washing of aggregates, the wash water will be treated by means of a filter press in order to extract the water again, which will return it to the washing process. The outcome is a filter cake with about 20% of remaining water. This material is, so far, dumped to the most part.

The applicability of these granite fines was tested several times in regard to various uses. Currently small quantities of granite powders are used in the calcium silicate block production, in ceramic applications as a grogging addition and even the applicability as an addition for the cement clinker production was studied. However, there is no mass application for this material, so far.

In literature the successful application of quarry waste materials for the production of SCC is reported (cp. [6] or [8]). Mostly this literature refers to dried and repulverized filter cake materials, which are as a matter of principle less interesting from the economic point of view, since their drying and grinding process requires much energy.

Above mentioned facts also apply for another rock flour type: a marble powder. These powders are contained in process slurry, originated during the processing of a Greek marble type, which is referred to as Thassos Limenas White (White of Limenas Thassos). It is a microcrystalline, dolomitic marble (marble powder A), quarried on the island of Thássos, Greece. Two other marble powders from this island have been introduced for additional tests on water demand and dry packing tests. These are a calcitic marble powder (marble powder B) and another dolomitic marble powder (marble powder C). The oxide-chemical description of both the granite and the marble powder can be found in Table 3.

2.1.3. Reactive powders

From the variety of mineral-reactive powders for mortar and concrete production, fly ash is attached with the greatest importance. For this reason two similar types of fly ash were involved in this study. In Table 3 the oxide-chemical composition of fly ash A is given.

In connection with some tests on the water demand of powders, namely the spread-flow test, three other reactive powders have been introduced. These are trass and two types of gypsum. Trass is, similar to fly ash, a pozzolanic material, which requires calcium hydroxide for its reaction. The two gypsum materials (gypsum A and B) are both α-hemi-hydrates which basically only differ in their fineness.

2.1.4. Model particles

For the modeling of dry packing experiments as well as paste flow experiments a model particle with ideal spherical shape is needed. For this purpose two different fractions of glass beads have been introduced. This is on one hand a fraction 0–50 μm and a 50–105 μm fraction on the other. Both have been characterized as very narrow fractions by using laser diffraction measurements.

2.2. Physical properties

In the following section the physical properties of the above introduced powder materials are determined.

2.2.1. Density

In the 8th edition of the Compilation of ASTM Standard Definitions one can find more than 40 definitions which refer to a mass per volume unit. In the publications of the British Standards Institute there are still 14 different definitions for densities mentioned. Correspondingly, the variety of available test methods is also immense.

The applied powders were tested according to EN 1097-7 using the pycnometer method. Hereby demineralized and deaerated water was used for non-reactive powders, and propan-2-ol for reactive powders. Before determining the total mass, the filled pycnometers always have been exposed to low vacuum for at least 24 h until no obvious release of air from the powder takes place anymore. The results of the density measurements can be found in Table 4.

2.2.2. Void fraction

All solid granular materials possess a certain percentage of their unit bulk volume as voids, i.e. the void fraction is defined as the proportion of void to the total unit volume and thus is dimensionless. This void fraction is depending on the particle size distribution, the particle shape, the applied compaction effort and the humidity of the considered fraction. The same holds true for mixes composed of individual granular bulks. Comparing the apparent bulk density ρ_{app} of a granular bulk with its non-porous specific density ρ_s, results in the respective packing fraction (P). The void fraction Φ, being representative for the current state of packing reads as:

$$\Phi = 1 - P = 1 - \frac{\rho_{app}}{\rho_s} \quad (1)$$

Thereby, the apparent density depends on the mode of packing. In powder technology it is common to distinguish void fraction both in loose and dense state. Focusing on dense state it still remains vague how dense packing can be applied. Within this research, dense void fraction therefore was further distinguished into vibrated and compacted void fraction. The measurement of the three apparent densities will be explained subsequently.

It should be noted that in the following the dry packing of particles is addressed. This gives information on the general compactibility of dry powders. However, these results cannot be applied to wet particles as we will find in concrete. This problem is addressed in a later section.

2.2.3. Loose packing

The achievement of loose packing is in practice difficult, since slightest influences can already lead to a compaction. Loose packing density, ρ_{loose}, or sometimes referred as freely settled density describes the lowest apparent density a bulk material can possess after being loosely piled. Therefore, tests on loose packing do not show as high repeat accuracy as tests on dense packing. For the determination of loose density and loose packing (or void fraction), a cylindrical container, similar to the one given in ASTM C 1252 (2003) but with slightly different volume has been applied. The respective volume of the cylinder is determined with a degassed liquid of known density. Deviating from the above mentioned ASTM standard, the container is filled via a decoupled, vibrated chute allowing shortest height of fall for the powder, and nearly a "grain by grain deposition". Appropriate deposition and free flow of the powder on the chute result in a loose volume of powder being almost free of compaction. This approach is assumed to be an improvement compared to the ASTM method which uses a funnel for the powder supply. The ASTM funnel has an opening diameter of 12.7 mm. Opening the outlet empties the filled powder jar at once. This results in compaction. The feeding of the cylinder has to be conducted until its intrinsic volume is filled. Excess heaped fine material needs to be stricken off carefully, again in order to prevent compaction. Using Eq. (1) the void fraction and packing

Table 4
Specific density of the powders and density properties in loose, vibrated and compacted state.

Material	Loose packing density, ρ_{loose} (g/cm^3)	Vibrated packing density, ρ_{vibr} (g/cm^3)	Compacted packing density, ρ_{comp} (g/cm^3)	Specific density, ρ_s (g/cm^3)
CEM I 52.5 R – micro-cement	0.804	1.072	1.720	3.15
CEM I 52.5 N	0.814	1.134	1.964	3.06
CEM III/B 42.5 N A	–	–	–	2.93
CEM III/B 42.5 N B	0.832	1.166	1.836	2.96
Limestone powder	0.848	1.154	1.846	2.71
Granite powder	0.659	0.980	1.694	2.72
Dolomitic marble powder A	1.011	1.323	1.974	2.80
Calcitic marble powder B	0.893	1.229	1.849	2.74
Dolomitic marble powder C	0.973	1.346	1.964	2.83
Fly ash A	0.885	1.155	1.628	2.21
Gypsum A	–	–	–	2.72
Gypsum B	–	–	–	2.72
Trass flour	–	–	–	2.50
Glass beads (fraction 0–50 μm)	1.396	1.530	–	2.42
Glass beads (fraction 50–105 μm)	1.463	1.539	–	2.46

now can be computed for the loose state. The results are given in Table 4.

2.2.4. Vibrated packing

Vibrated packing, also reported as tapped packing is achieved by filling the container with powder and exposing it to a specified compaction process, in this case vibration. Sufficient vibration is achieved when no more compaction occurs. The remaining volume is now filled with powder and again vibrated. This procedure is repeated till no compaction of the completely filled container is observed anymore. Thereby the intensity, frequency and duration of vibration are not critical [9]. The corresponding results can be found in Table 4.

2.2.5. Compacted packing

The void fraction of dry powders in compacted state is determined with a Rigden device according to EN 1097-4. The results for the compacted packing density can be taken from Table 4.

The wall effect, a general problem of determining particle packing in containers, does not notably influence the results of the three before mentioned packing tests as the mean particle size of the powder fractions is much smaller compared to the container dimensions. Therefore, the disturbed volume of the container becomes negligible. Ref. [9] refers in this regard to a container diameter which should be at least an order of magnitude larger than the applied particle size in order to obtain maximum packing density.

2.2.6. Analysis of packing experiments

Besides the specific density of a granular material, powders also posses an apparent density depending on their state of packing. The apparent density is the mass of powder particles divided by the volume they occupy. This volume can vary depending on the applied compaction. Based on this the terms loose, vibrated (or tapped) and compacted packing fraction, were introduced previously. From solid geometric considerations it is known that monosized, ideal spheres yield least packing if they are arranged according to the simple cubic (sc) packing, which results in a P of $\pi/6$ (about 0.52). But sc only serves as a model and does not occur during experiments as it is unstable [12]. Furthermore, if spheres are assembled by placing one sphere after another into a container, the models of regular packing cannot be applied anymore. Therefore irregular random packing becomes significant. For random loose packing (RLP) of uniform spheres at the limit of zero gravitational force, $\Phi_{loose} = 0.455 \pm 0.005$ prevails [10].

The two tested micro-glass bead fractions (0–50 μm and 50–105 μm, cp. Table 5) achieved void fractions in loose state of 0.42 and 0.40, respectively, which is almost the theoretical void fraction for RLP of monosized spheres. Furthermore, it is now generally agreed that random close packing (RCP), which represents the densest packing of uniform spheres having a random structure, amounts to 0.635 ± 0.005 [10]. This in turn corresponds to a void fraction of $\Phi_{close} = 0.365 \pm 0.005$. The achieved values from the vibrated close packed experiments show a void fraction of 0.37 for both glass bead types, which approaches the theoretical values. Note that no packing experiments for the compacted packing density have been executed with the glass bead fractions as it was assumed that the vibrated density already delivers closest packing for this spherical material. Furthermore, deformation and partial damage was expected for the glass beads under the impact of the piston in the Rigden device. However, both packing tests with glass bead fractions for RLP as well as for RCP showed a high correlation with the theoretical values and confirm the soundness of the modified test procedure introduced before. It should be once more noted that no uniform spheres have been applied, but narrow sized fractions. This is also confirmed by the results of a PSD measurement which is given in Fig. 1. All figures on the packing density and void fraction of the applied powder materials in varying state of compaction can be found in Tables 4 and 5. The void fraction is computed with Eq. (1).

Table 5
Determined void fractions in randomly loose, vibrated and compacted state computed with Eq. (1) based on the values given in Table 4.

Material	Loosely piled void fraction, Φ_{loose}	Vibrated void fraction, Φ_{vibr}	Compacted/dense void fraction, Φ_{comp}
CEM I 52.5 R – micro-cement	0.74	0.66	0.45
CEM I 52.5 N	0.73	0.63	0.36
CEM III/B 42.5 N B	0.72	0.61	0.38
Limestone powder	0.69	0.57	0.32
Granite powder	0.76	0.64	0.38
Dolomitic marble powder A	0.64	0.53	0.30
Calcitic marble powder B	0.67	0.55	0.33
Dolomitic marble powder C	0.66	0.52	0.31
Fly ash A	0.60	0.48	0.26
Glass beads (fraction 0–50 μm)	0.42	0.37	–
Glass beads (fraction 50–105 μm)	0.40	0.37	–

As can be seen from Table 5 the void fraction is reduced by applying vibration energy to the granular bulk and again during compaction in the Rigden device. For both processes a relation has been found, which describes the reduction of void fraction during compaction. In Fig. 2 the relation between the loosely piled void fraction and the vibrated void fraction is shown. From that it appears that there is a constant ratio between both void contents. Consequently the vibrated void fraction can be expressed by

$$\Phi_{vibr} = 0.842\Phi_{loose} \quad (2)$$

The above given correlation was found with good accuracy regardless of the shape of the applied particles. It can be seen that the three spherical materials, the two glass bead fractions and the fly ash A, achieved the lowest void fractions. The test results furthermore show that also angular particles, which is particularly the case for the applied cements and granite powder, can be reduced to the same extent in their void content like spherical ones.

Another correlation was derived comparing the vibrated void fraction with the compacted void fraction measured by the Rigden device. In this case the accuracy of the correlation was less since the micro-cement did not compact to the same extent like the other powders involved. It is assumed that from all the tested powders the micro-cement resists compaction the most, since its particles are angular and most of all the high fineness causes interparticulate forces, counteracting the compaction process. From Fig. 3 the following linear relation is derived:

$$\Phi_{comp} = 0.597\Phi_{vibr} \quad (3)$$

Now, using Eqs. (2) and (3) the loosely piled void fraction can be expressed as

$$\Phi_{comp} = 0.503\Phi_{loose} \quad (4)$$

Considering the fine micro-cement, as explained above, as an outlier, the correlation coefficient slightly improves. Now a correlation like shown in Fig. 3 is obtained. Thereby the factor between Φ_{loose} and Φ_{comp} changes slightly from 0.503 to 0.482.

As a modified method for the placing of powder particles into the container was applied, it is difficult to compare the obtained figures with values from literature. Brouwers and Radix [3] found a factor of 0.77 between loosely piled void fractions and close packing which corresponds to a void reduction of 23% during compaction. Most likely the herewith presented loose void fractions are higher than the values of [3]. Furthermore, they determined the packing in dense state based on the water content of paste

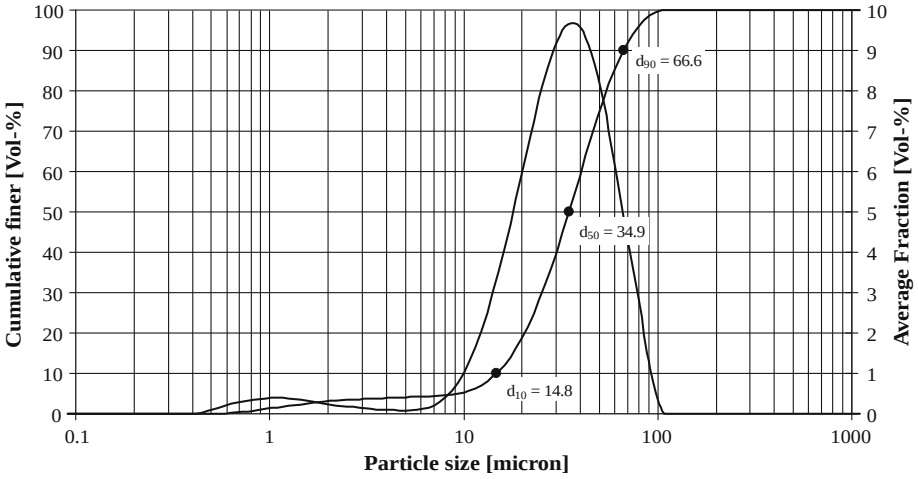

Fig. 1. Particle size distribution of the micro-glass bead fraction 0–50 μm. The narrow graduation allows comparative consideration with mono-sized sphere fractions.

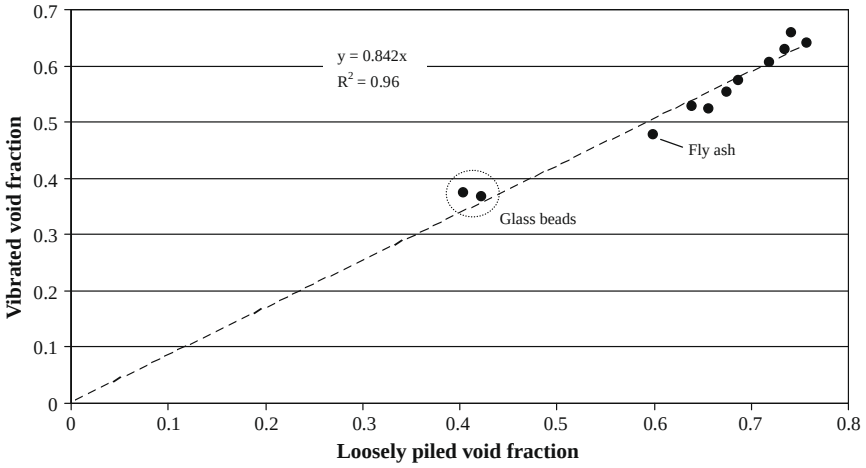

Fig. 2. Relation between the loosely piled void fraction and the vibrated void fraction.

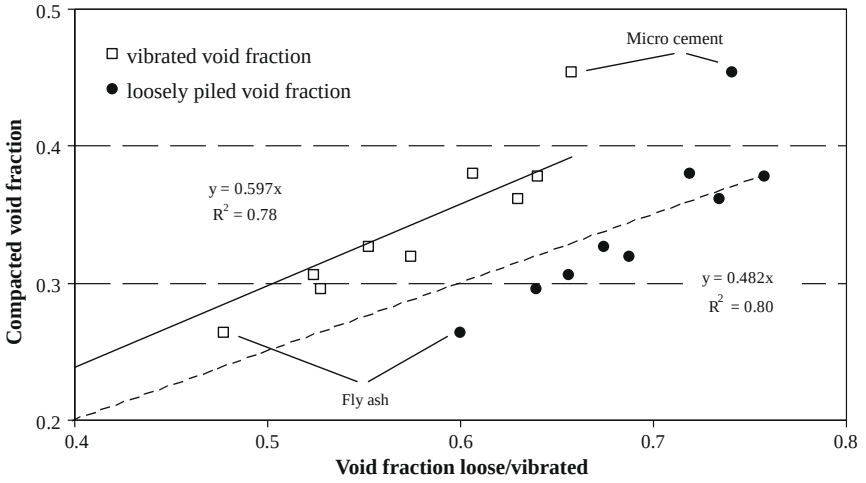

Fig. 3. Relation between the void fraction in loose or vibrated mode, and compacted void fraction.

(water–powder mixes) at the onset of flowing (as will be explained in a later section), which is not truly the densest state. Using this approach for the powders of this test series would result in a factor of 0.70, i.e. a void reduction of some 30% during compaction.

2.3. Granular properties

For the interests of concrete related powder analysis, granularity describes physical properties of the grain, such as particle size,

particle shape and the distribution of the particle sizes in the whole granular system. The particle size distribution (PSD) and particle shape of all involved materials of a granular mix have fundamental importance for the packing density of this mix and hence for the microscopic and macroscopic behavior of concrete mixes. Since the mix design tool, recently developed in the authors' research group [4], is based on continuous, geometric, random packing of all particles, granular powder properties attract special interest. In the following, the selected method of particle size measurement is described. Furthermore, the term specific surface area and its derivation are presented. Therefore, a computation model being based on a measured PSD is derived.

2.3.1. Particle size distribution

Measurement of particle size distributions is a major aspect of powder technology. There are numerous methods suitable for determining PSDs. Besides sieving and microscopy-techniques, most of the existing methods are based on either sedimentation of particles in suitable liquids or diffraction of light. Physical models are available, which help to analyze and finally turn the measured quantities into a PSD. Frequently however, their application appears to be problematic, which especially applies to the assumption of spherical shapes.

The deployed powder materials were measured using the low angle laser light scattering technique (LALLS), henceforth called laser diffraction. All powders have been measured in liquid dispersion with a Malvern Mastersizer 2000 using Mie scattering as measuring principle. For all powder types the Fraunhofer material model has been chosen as it does not require specific refractive indices for the individual materials. This setup is having two different light sources for detecting purposes, a red helium–neon-laser and a blue solid-state laser. The Hydro S unit was applied as wet dispersing unit. Thereby, non-reactive powders were measured using demineralized water as dispersion medium whereas propan-2-ol was deployed for reactive powders.

Since powder materials tend to agglomerate when being mixed into a liquid, particles need to be sufficiently dispersed in the liquid transport medium. In order to overcome the bonding forces on the surface of wetted particles, effective deagglomeration and dispersion methods are required. Ultra-sonication has been proven to be an efficient method. Exposing a suspension to ultrasound results in fluctuations of pressure and therewith in cavitation, which are in consequence generating microturbulences. Nevertheless, ultra-sonication should be carried out with caution since particles sometimes tend to reagglomerate during long-lasting ultrasound treatments. Furthermore, the pump velocity can also have an obvious effect on the obtained PSD. Therefore, experienced operators are required in order to achieve reliable results. Moreover, manifold additives are available in order to promote a deagglomeration of particles in the dispersing liquid. Their selection is depending on the type of particles to be measured. Polyphosphates such as sodium polyphosphates are often applied dispersants.

Measurement results on the particle size distribution of the selected powders are given in Fig. 4a and b.

2.3.2. Specific surface area

The specific surface area a, or SSA for short, is the quotient of the absolute available surface inclusive all open inner surfaces (pore walls) divided by the mass [m^2/g]. For concrete mix design, only the outer surface being in contact with water is of interest. With the consideration of the specific density, the specific surface area could also be expressed as area per volume [m^2/m^3], which here is denoted by S. Besides mass and solid volume the SSA also can be related to a bulk volume (taking account for the void fraction) or a cross-sectional area.

For the determination of SSA various direct and indirect measurement method are available. A widely known technique in cement industries is the Blaine test. This method is based on the pressure difference across a bed of dry and compacted powder, which is influenced by the flow rate and kinematic viscosity of air, the dimension of the bed of powder and its porosity. Applying this method, in general relative, rather than absolute fineness values are obtained. Hence a reference sample (e.g. calibration standard sand) with a given specific surface is recommended to use for calibration purpose. Establishing a steady state stream of air through the packed bed will result in the Lea and Nurse method. The more common Blaine method which is also available as automated variant, applies a fixed volume of air through the cell, which results in a steadily decreasing pressure rate. This can be handled easier than a constant flow rate [2]. Both tests give closely similar results but are not applicable to ultra fine powders or powders with higher fineness (particles < 10 μm). Furthermore, special attention needs to be paid to the preparation of the powder-bed since the assumed void fraction has to be achieved accurately. This fact demands for experienced operators. Another method that has been used to determine SSA is the volumetric static multi-point method by Brunauer et al. [11] better known as BET method.

2.3.3. Surface area computation

For the given powders no direct measurement of SSA was conducted but an indirect method was developed by using the PSD data. This approach was selected given that detailed PSD data of the powders is available anyway and there are no systematic restrictions in regard to the minimum particle size. Therefore, in contrast to Blaine, a SSA can be determined also for powders with high fineness.

An indirect possibility for determining SSA can be its derivation from the particle size distribution [12]. Assuming all particles are ideal spheres the derivation reads as follows. The volume V and the surface a of a sphere can be written as $V_{\text{sphere}} = (\pi d^3)/6$ and $a_{\text{sphere}} = \pi d^2$, respectively, taking d as the diameter of the sphere. The ratio of surface to volume, from the above two equations, then reads as

$$\frac{a_{\text{sphere}}}{V_{\text{sphere}}} = \frac{6}{d} \tag{5}$$

Assuming now a sample of particles with the uniform particle diameter d, the volume of the particles would then be m/ρ_s, where m and ρ_s are the total mass of the sample and specific density of the particles, respectively. Taking the volume of one particle, n, the total number of particles in the sample would read as

$$n = \frac{m_{\text{sample}}}{\frac{\pi \cdot d^3}{6} \cdot \rho_s} \tag{6}$$

Herewith the total specific surface area (mass-based) of the monosized sample is expressed as

$$a = n \cdot a_{\text{sphere}} = \frac{6 \cdot m_{\text{sample}}}{d \cdot \rho_s} \tag{7}$$

Considering the surface for a single fraction, derived via Eq. (7), the total specific surface of a granular material with known particle size distribution can now be computed. The particle size analyzer Malvern 2000 is giving values in the range of (theoretically) 10 nm up to 10,000 μm, using for the most part an increment factor of $d_{i+1}/d_i = 1.14815$, which is also called the diameter ratio u. This way a number of $n = 100$ fractions with $i = \{1,\ldots,n\}$ are created by $n + 1$ particle sizes d_i. The resulting diameter ratio characterizes a narrow range, which contributes to a realistic modeling of the PSD. With the help of Eq. (7) the surface area of each fraction i can be calculated, using the arithmetic mean of the particle sizes

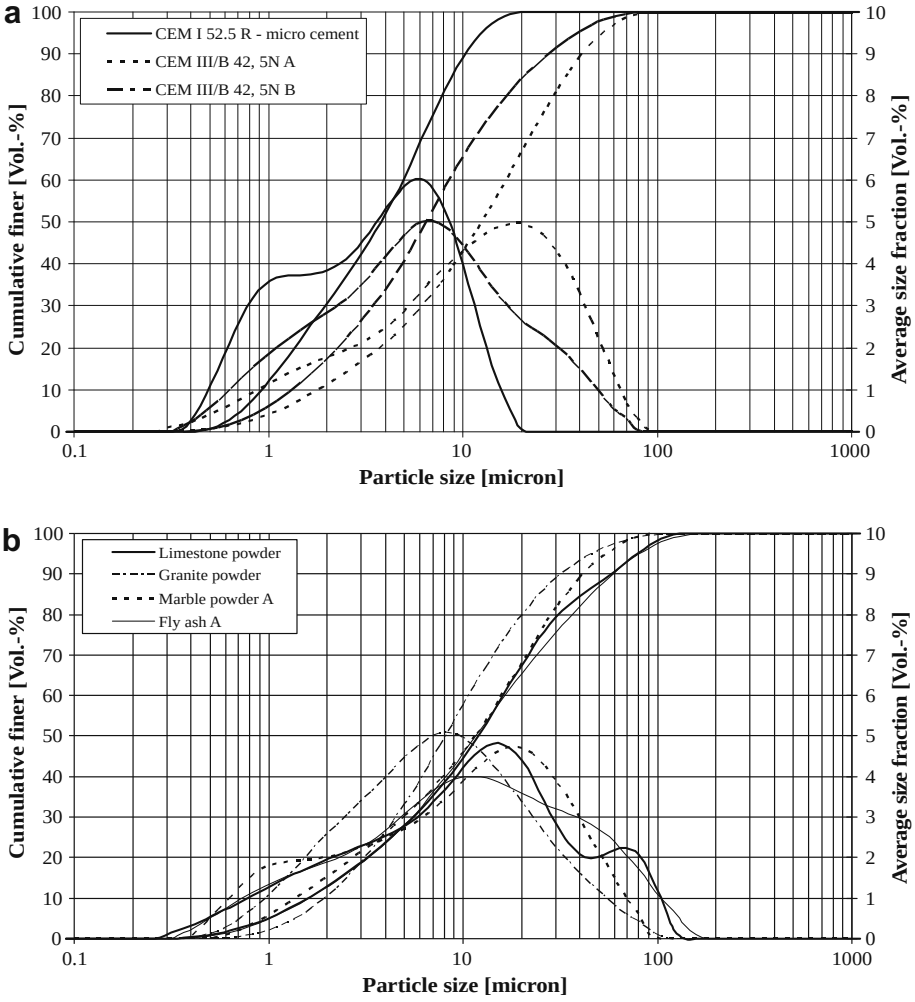

Fig. 4. (a) Particle size distribution of the selected cement types. (b) Particle size distribution of the selected powder types (excl. cement).

d_i and d_{i+1} of a fraction i as characteristic particle size. Hunt [13] is applying the arithmetic mean as well, whereas other authors use the geometric mean [14]. The arithmetic mean diameter $\bar{d}_{i,\text{arith}}$ of fraction ω_i is given with

$$\bar{d}_{i,\text{arith}} = \frac{d_i + d_{i+1}}{2} \tag{8}$$

Replacing the mass m_{sample} of the sample by the mass fraction ω_i of a grain fraction i, being the mass percentage of the fraction between d_i and d_{i+1}, the total specific surface of the single fraction i, reads as

$$a_i = \frac{\omega_i \cdot m_{\text{sample}} \cdot 6}{\bar{d}_{i,\text{arith}} \cdot \rho_s} \tag{9}$$

and consequentially for the whole sample as

$$a_{\text{sph}} = 6 \sum_{i=1}^{n} \frac{\omega_i \cdot m_{\text{sample}}}{\bar{d}_{i,\text{arith}} \cdot \rho_s} \tag{10}$$

Eq. (10) can also be found in [13]. Since a_{sph} is a mass-based measure, like the Blaine surface a_{Blaine}, the multiplication with the respective powder density, ρ_s, would turn it into a volume based specific area S, given in m^2/m^3. A summary of the computed specific surface area data is given in Table 6.

Given that mineral powder materials only seldom show ideal spherical particle shape, with silica fume being one of the few exceptions, a shape factor ξ has to be included in order to correct for the non-spherical shape. The corrected surface computation then reads

$$a = 6 \cdot \xi \sum_{i=1}^{n} \frac{\omega_i \cdot m_{\text{sample}}}{\bar{d}_{i,\text{arith}} \cdot \rho_s} \tag{11}$$

which can, besides [12], analogously be found in [2] and within the German standard DIN 66141.

In order to achieve a reliable SSA-computation an appropriate shape factor, which is independent of the particle size and only a function of shape, has to be selected. This will be explained later. Since specific density and particle shape of the powder materials are normally not constant for the whole range of particle sizes, this computation is approximate.

2.3.4. Characteristic size

In Eq. (9) the arithmetic mean is used as characteristic size of a fraction. Often the geometric means are applied as well. Computed surfaces based on arithmetic and geometric mean particle sizes of fractions differ depending on the size ratio of the selected fractions. The size ratio, u, is defined as

$$u = \frac{d_{i+1}}{d_i} \tag{12}$$

Using Eq. (12), Eq. (8) now reads

$$\bar{d}_{i,\text{arith}} = \frac{d_i(1+u)}{2} \tag{13}$$

Table 6
Surface area properties of the powders.

Material	Specific surface area					
	Blaine, a_{Blaine} (cm^2/g)	BET, a_{BET} (m^2/kg)	Computed sphere-based, S_{sph} (cm^2/cm^3)	Shape factor, $\xi_{Reschke}$	Computed non-spherical, S (cm^2/cm^3)	Computed shape factor, ξ
CEM I 52.5 R – micro-cement	–	2200	26,624	1.68	44,728	1.73
CEM I 52.5 N	–	–	15,749	1.68	26,458	1.57
CEM III/B 42.5 N A	4830	–	12,687	1.58	20,045	2.03
CEM III/B 42.5 N B	4500	–	17,775	1.58	28,085	1.36
Limestone powder	4040	–	13,850	1.26	17,451	1.22
Granite powder	–	–	13,051	1.50	19,577	1.26
Marble powder A	4580	–	14,739	1.50	22,109	1.16
Marble powder B	–	–	12,573	1.50	18,860	1.87
Marble powder C	–	–	13,391	1.50	20,087	1.29
Fly ash A[a]	2840	–	13,113	1.20	15,736	1.00
Fly ash B	–	–	13,419	1.20	16,103	1.09
Gypsum A	–	–	7970	1.80	14,346	1.30
Gypsum B	–	–	9713	1.80	17,483	1.18
Trass	–	–	15,603	1.20	18,724	1.10

[a] The fly ash is used as calibration standard for the shape factor computation.

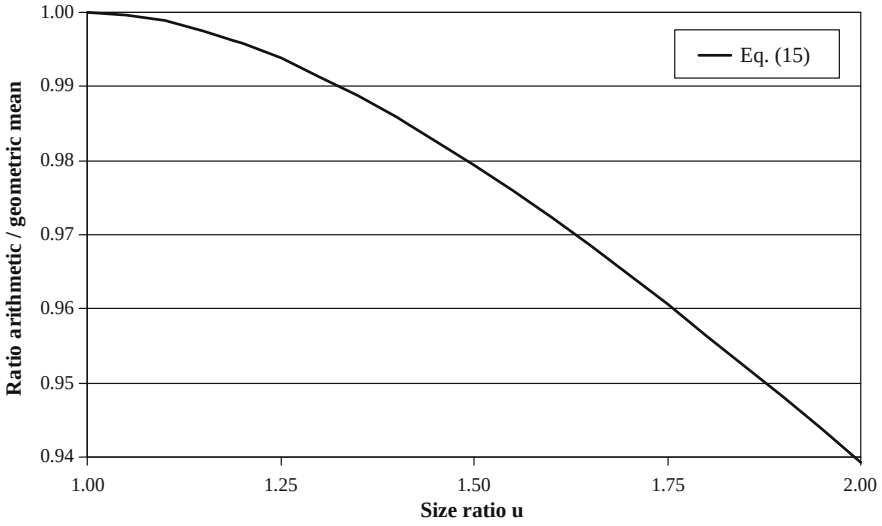

Fig. 5. Influence of an increasing size ratio, u, on the ratio between arithmetic and geometric mean, expressed as the deviation from unity. The location of the applied size ratio ($u = \sqrt{2}$) is indicated as well as the standard sieve set with $u = 2$.

Deploying Eq. (12), the geometric mean would read

$$\overline{d}_{i,geo} = \sqrt{d_i \cdot d_{i+1}} = d_i\sqrt{u} \tag{14}$$

Using Eqs. (13) and (14), the ratio between arithmetic and geometric mean now can be expressed as

$$\frac{\overline{d}_{i,arit}}{\overline{d}_{i,geo}} = \frac{1+u}{2\sqrt{u}} \tag{15}$$

Eq. (15) describes a variable factor between arithmetic and geometric mean based surface computations. It can be noted that the difference between both surface areas is increasing with rising size ratio u. Therefore, smallest possible increment values, like in this case $u = \sqrt{2}$, are preferable in order to keep the ratio close to unity (98%). When a size ratio of $u = 2$ is used, the deviation is still small (94%). Fig. 5 demonstrates the ratio of both sizes as expressed by Eq. (15). For this article the arithmetic mean is taken as representative size of a fraction. If one uses the geometric mean, the computed PSD can readily be obtained by using Eq. (15) in Eq. (11).

3. The water demand of powders

The water demand of powders, the finest particles in concrete, is a significant parameter for the design of concrete. It is composed of a layer of adsorbed water molecules around the particles and an additional amount needed to fill the intergranular voids of the powder system. Since powders provide by far the biggest part of the total specific surface area, they have the strongest influence on the total water demand of a concrete mix. Consequently, they should have a preferably low water demand. Therefore, an appropriate determination of the amount of water, needed to cover all particles with a water layer of a certain thickness is important. The water content is, besides the degree of hydration as well as cement type and amount, mainly responsible for the percentage of capillary pores, which is a direct indicator for the durability of concrete and mortars. An ordinary Portland cement only needs about 28% water related to its own weight for a complete hydration reaction. Furthermore, about 12% of water is physically bound in gel pores. This results in a water/cement ratio of about 0.4 for total hydration [2]. All water added in excess is only used to adjust

the workability of the mix, thus to lubricate the particles. Water demand, surface area, the resultant consistency, and the void volume are all related with each other.

There are different opinions on how the water demand of a granular mixture could be defined. Within concrete producing industry this term is often used to characterize a certain amount of water, necessary to obtain a specific consistency for a fresh concrete or mortar mix. Hence, the water demand depends on the desired consistency class and the deployed aggregate mixture considering its granular characteristics. In design codes there are tables given containing water demands for standard sieve lines. They are based on the required consistency and the grading value *k*. This value is a criteria applied to characterize the grading by concrete technologists in German-speaking countries. Analogous values are the fineness modulus Fm according to Abrams, the *F*-value according to Hummel and the cross-cumulative number (*D*-sum). The grading coefficient *k* is the summation of the oversize material (in vol.%) of the sieves 0.25, 0.5, 1, 2, 4, 8, 16, 31.5 and 63 mm divided by 100 [15]. This means that only the aggregate fractions are considered.

Furthermore, the amount of water needed for complete moistening of all particle surfaces is a possible description of the term water demand. Based on [16] this water is predominantly adhesively bound on the particle surface. For this declaration the target consistency is not important, only the dimension of the piled void fraction and the specific surface area of the particles are relevant.

In the strict soil mechanical sense the water demand or optimum water content is defined as the percentage of water at the point of highest achievable density, which is called maximum dry density [17]. This is for granular mixes only possible in partly saturated state, the so-called dry side, applying a specified compaction effort. Since surface tensions (capillary forces) are present, the free self-relocation of particles to the state of densest packing is hindered. This is also referred to as apparent cohesion. Achieving the saturation point the "capillary tension" disappears and the ternary system turns into a binary system. Now, having water in excess, the particles will fall apart and change the mix into a suspension. A saturated and undrained granular mix cannot be compacted since all compaction energy applied, is absorbed by the incompressible water. These effects are used for the Proctor compaction test which is going to be explained later on in this section.

Finally, another definition is available referring to the water content (β_p) of a powder material at the point where it starts to freely flow. This holds only for highly concentrated suspensions having water contents above the saturation point. The associated test procedure is the so-called spread-flow test.

This incomplete list of definitions for optimum water contents or water demands of granular mixes shows the necessity to exactly define the way, water demands have been determined, in order to understand the physical backgrounds and possibly different values. Due to the various definitions of water demand, there are also various ways to determine the related water content (also in variable accuracy). The following four test procedures, which are of special interest to the concrete producing industry, are going to be explained in more detail. Therefore, the term water demand is defined as the ratio of water and solids, unless otherwise noted, on volume basis.

Neglecting possible (minor) amounts of entrapped air, it is also possible to compute packing densities based on the derived water demands. A method for the determination of maximum packing density of dry particles was explained before. However, turning a fine granular dry mix into partly saturated state will change the interaction of particles. This can be explained by the various interactions of interparticulate forces. The characteristic maximum packing density of the dry state cannot be achieved anymore. These interparticulate forces interfere with the compaction of powders, both in dry and wet state.

In dry powder mixes interparticulate forces like van der Waals forces and electrostatic forces exhibit varying effects, depending on particle size. For small particles the theoretical adhesive force, as a result of the above mentioned forces, can be much higher than the particle weight, depending on the size. Therefore, fine powder particles adhere to another and as a result the mobility of individual particles is restricted, i.e. with increasing fineness of powders their compactibility is reduced. However, with appropriate surface additives (admixtures) adhesive van der Waals forces can be effectively reduced so that electrostatic repulsive forces become relatively dominant.

In presence of water, which is the case for powder suspensions, the van der Waals forces only have significance for small particle distances. With increasing distance resulting from the position of particles within the suspension (water layer thickness), the van der Waals forces decrease rapidly. The effect of electrostatic repulsive forces is in this case of significantly higher importance for the mobility of particles. These forces counteract the van der Waals forces and hence prevent particles from agglomeration [18]. Therefore, the position of particles within the suspension as well as the stability of the suspension itself and their rheological behavior are depending on the relation of electrostatic to van der Waals forces.

Therefore, the determination of water demands also serves as a method to test the packing density in wet state which represents the later conditions in concrete. As no method has become generally accepted for the determination of maximum packing density of wet particles different tests on the water demand of powders are introduced and analyzed.

3.1. The spread-flow test

The spread-flow test (or sometimes referred to as paste line test or mini-slump flow test) according to Okamura and Ozawa [19] appears to be the classical method for the determination of the water demand of powder materials involved in SCC. Thereby suspensions are produced being composed of the powder to be analyzed and varying quantities of water. After appropriate mixing following a defined mix regime, the suspension is filled in a special conical mould in the form of a frustrum, the Hägermann cone (cp. Fig. 6), which is lifted straight upwards in order to allow free flow for the paste without any jolting. In contrast to several literary sources (e.g. [20]) the obtained paste is not filled in two layers with intermediate compaction but in one into the cone, as its flow behavior solely due to own weight is going to be analyzed. This therefore also holds for the compaction. The recommended working surface for this test is a dry, clean, horizontal and non sucking surface (best is a glass plate). From the spread-flow of the paste, two diameters perpendicular to each other (d_1 and d_2) can be determined. Their mean is deployed to compute the relative slump (Γ_p) via

$$\Gamma_p = \left(\frac{d}{d_0}\right)^2 - 1 \,\text{with}\, d = \frac{d_1 + d_2}{2}, \tag{16}$$

where d_0 represents the base diameter of the used cone, 100 mm in case of the Hägermann cone. The relative slump Γ_p is a measure for the deformability of the mixture, which was originally introduced by [19] as relative flow area *R*. An example of an analyzed spread-flow test is given with Fig. 7.

3.1.1. Test procedure

For the production of the paste an ordinary mortar mixer for laboratory purposes with respective mix paddle according to EN 196-1 (1994) is used. The amount of paste to be produced has to

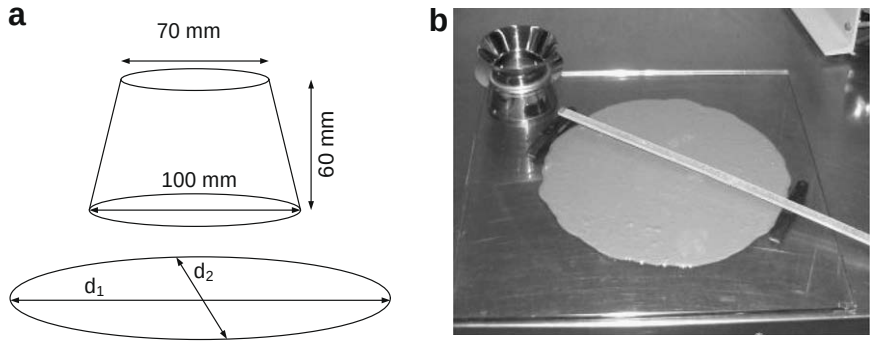

Fig. 6. Schematic of a spread-flow test. A: proportions of the Hägermann cone, B: Example of an executed spread-flow test with a marble powder, showing the Hägermann cone with filling hopper according to EN 459-2.

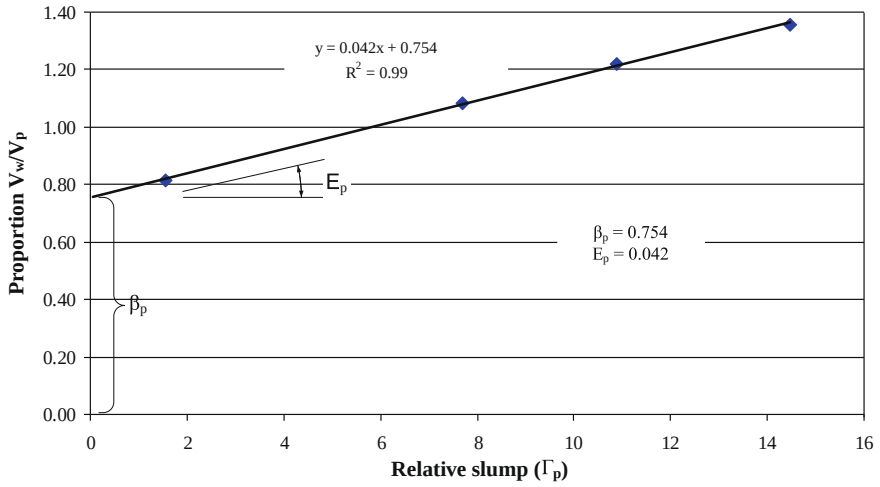

Fig. 7. Principle of a spread-flow experiment, showing varying water/powder proportions as a function of the relative slump flow.

be selected considering the type of mixer and volume of the applied cone. It should be assured that the mix is homogeneously mixed and that the cone can be filled twice. The applied mix procedure is given as follows:

- Adding the weighed amount of water into the moisturized mixing bowl.
- Continue with adding the complete amount of powder.
- Start mixing for 30 s on speed level 1 (140 ± 5 rpm).
- Stopping the mix activity for 60 s, where the first 30 s are used to scratch splashed material from the wall of the mixing bowl and the paddle.
- Continue mixing for further 90 s on speed level 1.

The paste, prepared in this way is filled in the dried and cleaned Hägermann cone using a filling hopper. After filling, the hopper will be removed and surplus material is wiped off to ensure using an equal volume of material every time. This is followed by straight lifting the cone whereupon the paste spreads over the flow table. After cleaning of cone and flow table the spread-flow test is immediately repeated using the same material again in order to derive two mean diameters for one water/powder-ratio, i.e. four individual diameters for one water/powder-ratio. At least four different water/powder-ratios have to be tested to obtain a statistically reliable trend line. Thereby, new water/powder-ratios are realized by preparing new mixes following the above described procedure and explicitly not by adding water to the present mix. It is furthermore recommended by [21] to aim on spread-flows of 140 mm up to 230 mm, which corresponds to a relative slump Γ_p of 0.96–4.29 using the Hägermann cone. Other literature refers to a range from 0.2–15 [20]. It is believed that any spread-flow can be accepted for assessment, as long as it shows a measurable and symmetrical spread, and possesses no signs of segregation (obvious centric pile) or bleeding (corona of bleeding water).

3.1.2. Result analysis

By means of a graphical analysis (cp. Fig. 7) all measured Γ_p are plotted versus their respective water/powder volume ratios (V_w/V_p) involving the respective specific densities of the deployed materials. A straight line is fitted through the derived data points afterwards. The intersection of this linear function with the axis of ordinates at $\Gamma_p = 0$ depicts the retained water ratio where no slump takes place [22]. In other words, this denotes the maximum amount of water which can be retained by the particles. Exceeding this water content will turn the coherent bulk into a concentrated suspension. This point is referred to as water demand or retained water ratio, which was introduced as β_p in the field of concrete.

From the measurement, a linear relation can be computed for each material with the help of linear regression. The outcome of this analysis is a function of the type

$$\frac{V_w}{V_p} = E_p \Gamma_p + \beta_p \tag{17}$$

Besides the water demand β_p, information is also provided by the value E_p, the deformation coefficient, which is the slope of the function. This value can be understood as a measure of sensitivity on the water need for a specified flowability. That means materials showing a lower E_p, hence having flat slopes, respond

with bigger change in deformability to a certain change in water dosage than materials having a steeper slope. Thus small changes in the water content have a stronger influence on the relative slump. In this way, materials can be identified that tend to bleeding or segregation sooner than other materials in mortars and concrete mixes. The probability of this negative behavior becomes higher with decreasing amount of cement and with high amounts of powder materials exhibiting strong sensitivity to water changes (low E_p-values).

3.2. The Puntke test

This test method was developed by Puntke already in the 1960s for a rapid testing of fly ash. In the meantime this method became standard test procedure of the German fly ash suppliers and it is also used for the determination of fine materials' water demand. Furthermore, this test is in preparation to be included in the German guideline for self-compacting concrete [23].

The execution of the Puntke test will result in the water content at the point of saturation, which depicts the transition from a coherent packing to a suspension. Therefore, a fine, cohesion-free granular skeleton cannot be self-compacted to a specific packing density until the water content is sufficient for the saturation of the dense grain structure. For this reason the test is only influenced by the water content and not by an accurately defined compression process. Under the impact of water saturation the capillary tension of the powder bulk disappears. Now a rearrangement to the densest packing in the state of saturation is possible. This results in a reduction of the loosely piled void volume, which immediately turns the system into a supersaturated state. In practice this would lead to segregation and bleeding of the paste. These first signs of bleeding are a shining surface of the water–powder mixture, which also is the evaluation target criterion of the addressed test. The density achieved herewith is indeed not the maximum density. The latter can only be found on the dry side in partly saturated state applying compaction to the system.

3.2.1. Test procedure

A cylindrical plastic or metal beaker with planar base and a volume of circa 100–300 ml is filled with test material (50 g for powders, 100 g for sand) and weighed. With the help of a wash bottle water is added in very small steps. After each addition of water the mass has to be mixed by hand with an appropriate tool, e.g. a stir spattle. Afterwards the beaker is stamped by falling from about 5 cm height a couple of times. When the mix shows a closed structure and brilliance on top, the saturation point is achieved. The required quantity of water can now be determined by weighing. The addition of water has to be executed carefully with a pipette or a wash bottle, close to the saturation point even dropwise [23].

3.2.2. Result analysis

Puntke assumes that for the point of saturation the granular blend becomes free of air, i.e. the void fraction is completely filled with water. Based on that, Puntke derives a relation between the void fraction Φ and the involved volumes of water and powder represented by their masses. This also allows the determination of the water demand and the computation of the void fraction. The corresponding equation reads as follows

$$\Phi = \frac{V_w}{V_p + V_w} = \frac{\frac{m_w}{\rho_w}}{\frac{m_p}{\rho_p} + \frac{m_w}{\rho_w}}. \quad (18)$$

The specific density of the water is taken to be 1.00 g/cm^3 (0.9982 g/cm^3 at 20°C). In this way the void fraction in the state of saturation can be determined. The specific density of the tested powders can be found in Table 4.

3.3. The Vicat needle test

The Vicat needle test is known from cement industry. It is about the determination of setting time of cement pastes. Although this test was the first measurement on setting time in the 19th century, when concrete became more widely introduced, it still remains the most used test by the cement manufacturing industry [24]. Therefore, it is subject of various standards (e.g. EN 196-3, ASTM C191-04b or BS 4550-3). However, this test also gives an indication for the norm stiffness of cement paste, which is depending on the water content of the paste. Besides cement pastes this test is applicable for other powder materials and fine sand.

The physical background of the test is based on the resistance of a paste to the penetration by a rod with a certain weight and shape (shear strain). It is furthermore supposed that stiffening during the set generates a gradual increase in resistance to shear.

3.3.1. Test procedure

For the realization of the test, a paste with a certain water/powder-ratio has to be prepared by following the mix regime defined in EN 196-3. Thereby, the powder has to be added to the water in the mixing bowl within a time frame of minimum 5 s and at most 10 s, in which the end of the powder addition is set as the zero time. The ready mixed paste is filled in a conical mould and centered below the dive rod of the Vicat needle device. In doing so the undersurface of the rod has to be fixed on top of the paste surface such that they touch each other. Exactly 4 min after starting the mix process (zero time) the rod has to be released from its anchorage to penetrate the paste. On a scale one can read the depth of penetration or rather the distance from the undersurface of the rod to the base plate (inverse scale). This distance is the test criterion. The test has to be repeated with diverse water/powder-ratios until a value of 6 mm is obtained. A paste satisfying this criterion is supposed to have normal (standard) stiffness and, at the same time to show the water demand needed to obtain this normal stiffness.

3.4. The modified Marquardt test

A more recent test for the determination of water demands is described by Marquardt [16]. This test is suitable for powder materials, mortar mixes and, adequate equipment presumed, also for entire concrete mixes.

Marquardt characterizes the water demand as the percentage of water, adhesively bound on the particle surface. This water fraction can be determined via the standardized power consumption of a mortar mixer during the mixing process while adding water. The basic principle behind this test is the resistance to shear stress of pastes with different moisture contents. A dry powder would only confront the mixing process with a low shear resistance resulting in low power consumption. However, adding water in little amounts to the mix (incremental or continuous), would increase the power consumption to a maximum due to agglomeration of individual particles. This obvious maximum in the power consumption graph reflects the water content where all particle surfaces are wetted and the particles themselves are connected via water films. Further adding of water leads to a liquefaction of the mix. The power consumption of the mixer will decrease due to the increasing thickness of water layers around the particles. Fig. 8 is illustrating this phenomenon.

3.4.1. Test procedure

The execution of this test does not require for special apparatus. A standard mortar mixer and equipment displaying the power consumption of the mixer are sufficient. Ideally, this data on the power consumption should be digitally available to permit processing of the data. For this research a digital multimeter was deployed to

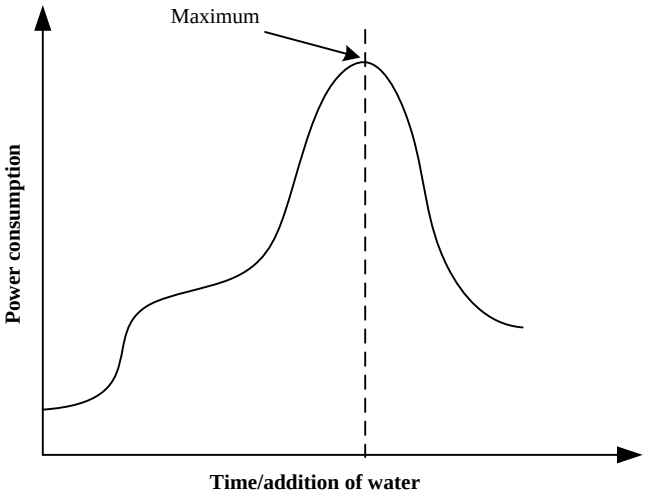

Fig. 8. Process scheme about the development of the power consumption of a mixer as a function of the addition of water.

display the current consumption of the mortar mixer. Before mentioned multimeter is having a power adapter, a device to be connected between power outlet and mixer, for this purpose. The multimeter again possesses an interface in order to collect the data with a computer.

Similar to standard mortar tests, a wall-wetted mixing bowl is used in order to prevent the wall adsorbing water from the mix. This bowl is filled with the material to be tested and subsequently is fixed to the mixer. For a standard mortar mixer amounts from 1000 g up to 3000 g of powder are recommended in order to achieve a sufficient filling level of the mixer. Water demands determined for powder dosages below this minimum amount could be sensitive to changes in the powder load.

The mixing process and recording of data are started simultaneously and after homogenization of the mixture a constant power consumption will be obtained. Then, the addition of water is started. According to [16] a constant water supply of about 1.5 ml/s has to be dosed. The starting point of water addition has to be annotated since the effective, actual water content is not measured but later computed by the time needed to achieve the maximum in power consumption. Adding water to the dry granular bulk will first fill bigger cavities and cracks in the particles, and the intergranular voids. This will not be responded with a sharp rise of the power consumption. However, due to increasing agglomerations of individual particles the power consumption will increase up to a maximum, which is caused by complete water layers of a certain thickness around particles raising adhesion to a maximum. Further addition of water finally leads to a decline of the mixer engines' input power. This is explained by increasingly thicker water layers around particles lowering the shear forces needed to mix particles by increasing the distance of particles. In principle, this is similar to the Puntke situation at highest density. Therefore, the Marquardt test is expected to provide similar figures like Puntke. After liquefaction of the mix, the procedure can be stopped. Finding the maximum power consumption will at the same time lead to the associated water content.

3.4.2. Observations and modifications

While conducting this test, it was observed that the response of the power consumption to water additions was delayed by about 10 s, which corresponds to the time, the water first needs to be homogeneously dispersed in the mix. Hence, applying a water supply with a flow rate of 1.5 ml/s would result in water demands overrated by approx. 15 ml. This in turn corresponds to a deviation of 1.5%, assuming an amount of 1 kg of dry material. It was therefore decided to first use an incremental water supply instead of a continuous addition and secondly, to apply a two-stage process having a: (i) rapid, rough determination followed by a (ii) finer detailed measurement step. For the first orienting measurement (i) an initial amount of 1000 g dry powder is mixed with water in steps of 10 ml every 20 s. Now having an indication for the water demand, the next more detailed measurement step (ii) can already be started with the assumed water demand lowered by approx. 15 ml. Then the same procedure is recommended but adding 1 ml every 15 s. In doing so, it is important to first sufficiently homogenize the mix with the initial amount of water. The stepwise addition of water should only be started when the power consumption has been stabilized. An example of the small step procedure is given in Fig. 9.

3.5. Alternative methods

In addition to the above mentioned tests there are also alternative test methods for the determination of water demands available.

On example is the centrifugation of moisturized aggregate fractions. By the comparison of the dried and wet centrifuged aggregate weight, the amount of water on the surface is computed. This amount is equivalent to the water demand of the fraction and is also related to the total aggregate surface [16].

Centrifugation can also be applied to powders. Hereby, a suspension made from powder and water is poured into suitable centrifuge tubes. After centrifuging, the clear top layer of water is decanted and by means of weighing, the amount of water is determined for the remaining paste.

Another possibility is the derivation of the optimum water content by means of the Proctor compaction test. This test method is known from soil mechanics but its principles can also serve the needs in concrete technology. Therefore, this test is mostly applied in a modified variant, whereby the modifications regard the procedure of filling the Proctor mould or the way of compacting the sample. For the readers interest, it is referred to the modified Proctor variants which are applied in the STEAG-method ([25,26] or [27]). Recently, the Proctor test was applied by Fung et al. [28] in the so-called wet packing method.

3.6. Results on water demand

The four different test methods introduced before have been applied to the selected powder types listed in Table 4. A comparative description of the results is given with Table 7 and is illustrated in Fig. 10. The experiments are mass-based, and have been expressed in volumes by using the specific density of water and powder concerned (cp. Table 4). It should be once more noted that the water demand represents water/powder ratios on volume basis.

Analyzing the data, it turned out that Puntke and Marquardt always yield the lowest values, with Puntke being slightly smaller than Marquardt. A good correlation between both measures, having a factor of 0.96 shows, that both values can be almost directly translated into each other (cp. Fig. 11a and b). Lowest water demands for the Puntke test were expected, as it is the only test method within this series where a granular bulk is densified by applying compaction effort. Furthermore, the expected small deviation between Puntke and Marquardt results was proven by experiment.

The analysis of the Puntke method resulted in some questions; namely that this method has low comparability and is not completely coherent. Puntke [23] assumes to determine the water content for a mixture with minimum void content in complete saturated state. From soil mechanics it is known that minimum

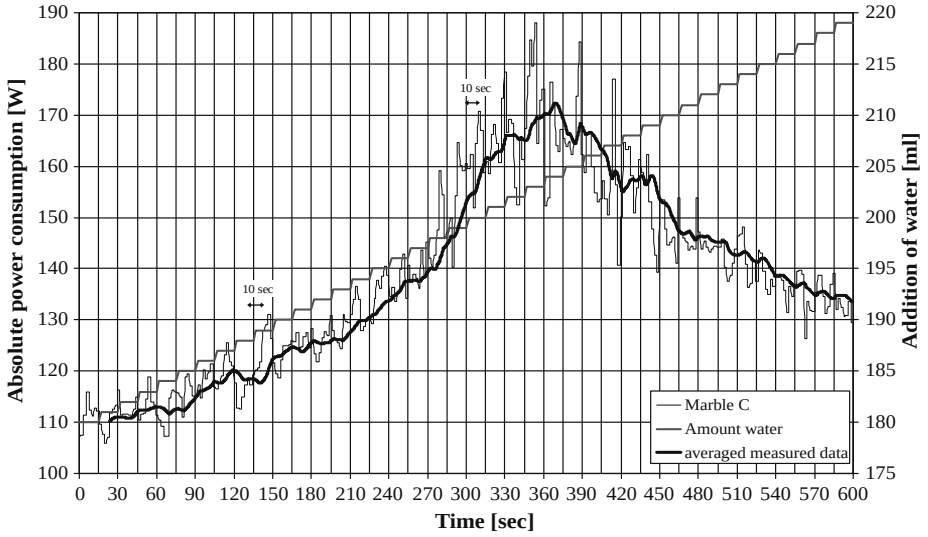

Fig. 9. Development of the absolute power consumption during incremental addition of water (1 ml each 15 s) to a specific marble powder. The bold graph shows the smoothed measured data.

Table 7
Comparison of the volume based water/powder-ratios derived by the different test methods.

Material key number	Volume based water/powder-ratios			
	Puntke	Marquardt	Paste lines	Vicat
CEM III/B 42.5 N A	0.791	0.791	0.976	0.878
CEM III/B 42.5 N B	0.782	0.877	1.241	–
Fly ash A	0.464	0.486	0.532	0.502
Limestone powder	0.548	0.603	0.762	0.627
Granite powder	0.627	0.659	1.215	0.768
Marble powder A	0.560	0.588	0.874	0.686
Marble powder B	0.637	0.620	1.005	0.631
Marble powder C	0.577	0.577	0.829	0.735

void content, what again means maximum density can only be achieved in partially saturated mixtures being a ternary system from soil, water and air. Therefore the void fraction, derived by Puntke, is still subject to error, since only the water content is considered but no air fraction being present at the point of highest density. The practical execution of the Puntke test has shown that the applied compaction effort is influencing the obtained water demand. Instead of tapping the beaker it is recommended placing the sample for e.g. 15 s on a vibration table, in order to expose it to a defined amplitude. This makes the procedure quicker and the test becomes more reproducible since the placed compaction energy is always the same. The fact, that sometimes a tapping of 20 times leads to apparent saturation, whereas in other cases this point can only be obtained after 80 times caused the search for a verification of the method in this respect. In other words the "several shocks" mentioned by [23] need some more explanation.

Within this analysis another correlation was found, namely between the modified Marquardt method and the Vicat test, known from cement characterization. Their relation is given in Fig. 11. In average the Vicat measures turned out to be about 10% higher than the Marquardt water demand, which corresponds to the range of 8–10% mentioned by [29]. However, the Vicat results only show low significance in the framework of these tests. As the Vicat test does not show that high accuracy as the other three tests explained, the Vicat test is not recommended for these kinds of experiments which demand for reproducible and reliable results. Moreover, Marquardt's conjecture [29] that her approach delivers lower values than Puntke could not be confirmed by experiments, as discussed above (see Fig. 11a). In the later literature, besides this assumption, no further measurement data is available to the authors' knowledge.

As expected the spread-flow tests always led to the highest water demands within this investigation. In contrast to Puntke and Marquardt test, where saturation conditions are approached, the spread-flow method yields namely a water content which characterizes the transition of a saturated granular bulk into a suspension, i.e. the onset of flowing.

With the spread-flow test, the classical approach of determining the water demand for self-compacting concretes is included. It has been shown that a granular solid mix can, after exceeding the point of saturation (Puntke test) and the state of maximum shear resistance (Marquardt test), retain water in the structure till it starts freely flowing under only its own weight while increasing the water content.

Besides the correlation between the modified Marquardt method and Puntke, and the modified Marquardt method and Vicat test, the Marquardt results also were correlated with the spread-flow experiments. The correlation can be seen in Fig. 11b.

By [3] the E_p and β_p of the spread-flow test were used to put two hypotheses forward. First a relation was derived between the amount of water that can be retained and the void fraction of the powder (β_p). Furthermore, another relation was derived between the slope of the paste line (E_p), and the internal specific surface area of the powder. Here, E_p and β_p are used to validate these two hypotheses using a specific surface area derived in a different way. Moreover a shape factor will be derived on this basis to correct powder particles for their non-spherical shape. This will be presented in the next section.

4. Analysis of flow experiments

4.1. Derivation of a shape factor based on flow experiments

In the following the derivation of a shape factor, based on flow experiments with water–powder mixtures, is described. This procedure will indirectly provide a shape factor, not being based on direct measurements of particle dimensions, but relevant for water–powder flow.

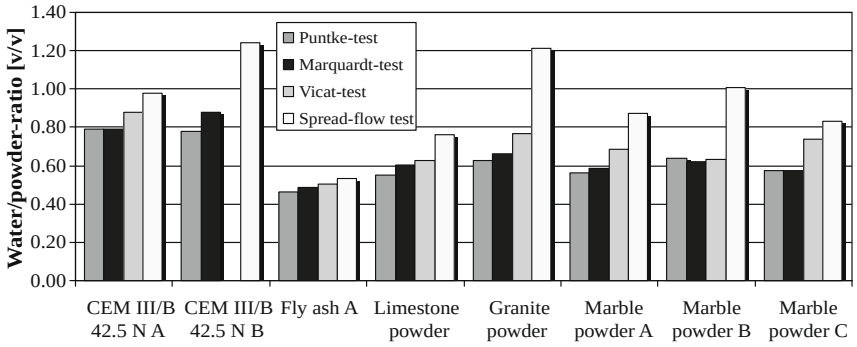

Fig. 10. Comparison of the volume based water demands derived by the different test methods, values taken from Table 7.

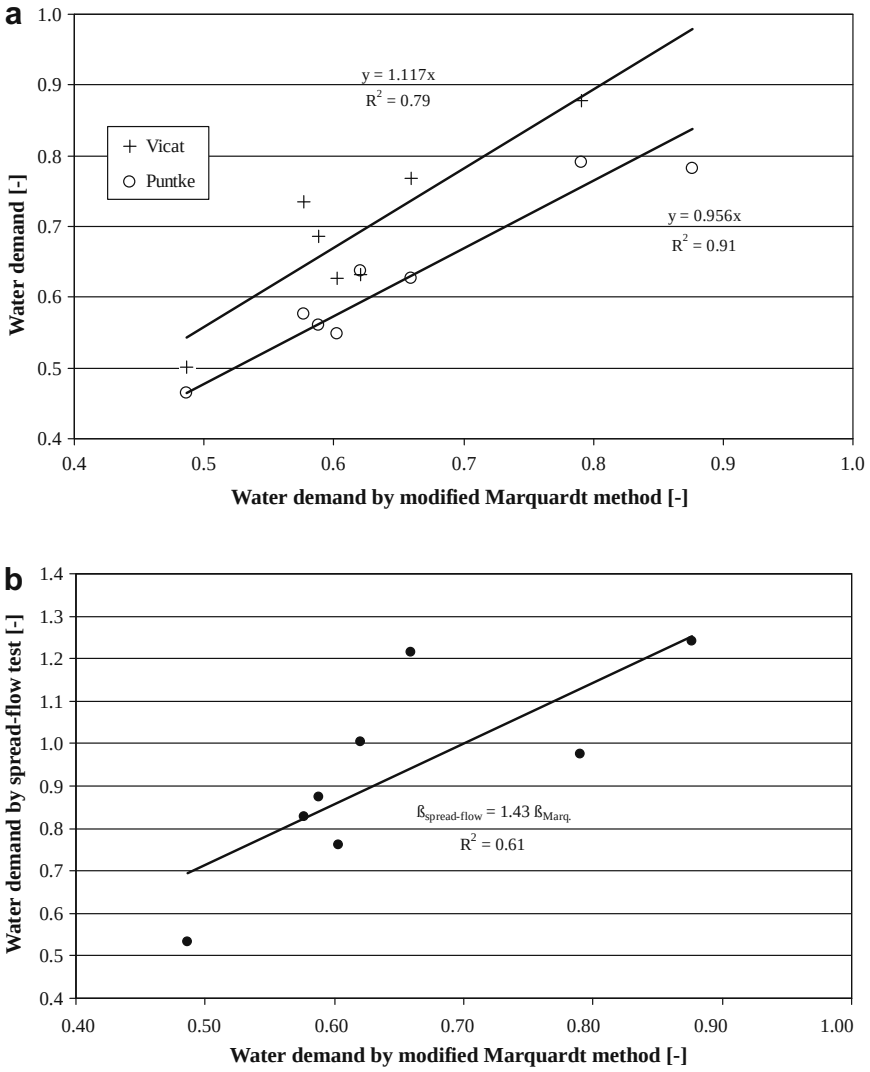

Fig. 11. (a) Correlation of volume based water demands derived by Puntke and Vicat test as a function of the modified Marquardt method, values taken from Table 7. (b) Correlation between Modified Marquardt method and spread-flow experiments, values taken from Table 7.

The shape of particles is a complex function of their formation conditions, the mineralogical composition and particle size. Since most of the powder materials applied in concrete industry are of artificial nature or at least processed by e.g. milling, the lithology, the mode and duration of transport as well as the nature and extent of post-depositional weathering, which are important in sedimentology, are only of minor relevance.

The particle shape factor is expressing the ratio of an effective particle surface area of an irregularly formed particle to the surface area of an ideal sphere with equal volume. According to this definition, the ideal, smooth sphere would have a shape factor, ξ, of 1. This represents a three-dimensional approach, being based on volume considerations. In principle two approaches are reported in literature. On the one hand two-dimensional particle shape

measurements are conducted with the help of images or projections. On the other hand three-dimensional analysis with individual particles is possible by measuring the principal axes of an irregularly shaped particle. Both approaches are direct measurements as specific geometrical characteristics of a particle are considered.

Besides the classical approach of directly measuring particle dimensions there are also indirect ways to derive an overall shape factor. The above described methods provide a number of measures, which can describe particles in detail. However, their combination to an overall shape factor turned out to be difficult. Motivated by the varied usage of shape factors, there is an interest to find suitable values with more general measurement techniques or in other words to find correlations with values measured anyway. One approach was for example given by Reschke [30], who is forming a ratio of the directly measured Blaine surface a_{Blaine} and the computed surface area a via

$$\xi_{\text{Reschke}} = \frac{a_{\text{Blaine}}}{a} \tag{19}$$

The computed surface area a was thereby developed from the particle size distribution measurement using laser diffraction and assuming spheres, similar to the procedure described in Section 2.3. So, [30] used Blaine values to calibrate and derive shape factors. Therefore, the obtained shape factors still contain the systematical error involved with the Blaine measurement. Subsequent to the computation of the shape factors their plausibility was verified by SEM-documentation of selected powder materials. Analyzing the results obtained, groups of similar materials were formed when organizing the shape factors in ascending order, i.e. generalized each material type is forming narrow ranges of shape factors.

In total Reschke determines a range of shape factors ξ_{Reschke} from 1.00 up to 3.08, of which 1.00 represents micro-glass spheres and 3.08 a kaolin type. However, the value for the micro-glass spheres was not measured but assumed to be unity. Therefore this model cannot be considered to be aligned with the ideal model case. Summarizing, this model gives plausible results being in line with the SEM-image analysis.

In order to compute specific surface data with the approach derived in Section 2.3, the particle shape data provided by [30] was, for the time being, used to correct the computed surface area for the particle shape. In the following, a model for the computation of shape factors will be derived based on flow experiments. Then, these values based on Reschke are used for comparative purposes. In Table 6 the selected shape factors are given in combination with the sphere-based surface area, as well as with the shape-corrected surface area.

One of the major hypotheses put forward by [3] was that the relative slump of a water–powder mixture becomes a function of the specific surface area when sufficient water is present for flow, i.e. $V_w/V_p > \beta_p$. This hypothesis was validated by relating the slope of the spread-flow function E_p (cp. Eq. (17)), the deformation coefficient, to the specific surface area S. The specific surface area taken from Blaine (a_{Blaine}) was multiplied by the specific particle density ρ_s to obtain the specific area per volume of powder. From the observations it was concluded that the larger the internal surface, the larger the deformation coefficient (the more water is required to attain a certain relative slump). Accordingly, the following linear relation was derived:

$$E_p = \delta \cdot a_{\text{Blaine}} \cdot \rho_s = \delta \cdot S, \tag{20}$$

with δ representing the thickness of an idealized water layer, surrounding the particles of a water–powder dispersion with $V_w/V_p = \beta_p$, i.e. the onset of flowing. [3] found a mean δ of 41.32 nm. This range was also confirmed by [16], who found a layer thickness of about 150 water molecules for the water demand of particle fractions by means of sorption experiments. This layer thickness corresponds to approximately 45 nm as the size of one water molecule is about 3 Å.

In this section the above approach is applied for the derivation of a shape factor, considering a larger number of powder samples. A further modification is introduced by the substitution of the Blaine surface area by the uncorrected, computed specific surface area a_{sph}, derived with Eq. (10). This PSD-based computed surface area is a weight-based measure like the Blaine surface too. The PSD-based surface area is chosen since the Blaine measurement holds some uncertainty in itself, especially for powders of high fineness, since the Carman–Kozeny equation used in air permeability method is not valid for particles smaller than 10 μm [13]. In principle the computational models for laser diffraction and the measurement itself also contain some inaccuracy, but no systematical error is additionally introduced, as would be the case by using Blaine measurements. Since the derived shape factor will later be applied on the detailed PSD, containing the same systematical error, there will be no multiplied effect on the corrected computed surface area. Furthermore, the PSD data is available and Blaine does not need to be determined in addition. Blaine test and computed surface area both describe the outer surface of particles and apart from a systematic deviation due to different measurement principles they provide basically the same information. This is also confirmed by Robens et al. [31].

Now, plotting the computed specific surface area (S_{sph}) of these powders against the deformation coefficient E_p, Fig. 12a is obtained. Table 8 provides the necessary results of the spread-flow tests on these powder materials. Note that E_p, β_p and S_{sph} used in this graph are all volume based, and S_{sph} is the specific surface if the particles were truly spherical. With the help of linear regression a relation was derived for these measures. Based on the assumption that the slope of a paste line becomes a function of SSA when $V_w/V_p > \beta_p$ is satisfied, the regression line has to intercept the point $E_p = 0$. Now, assuming straight lines from every data point through the origin would result in lowest slopes for the two fly ash powders involved, the two materials with the most spherical shape. Their true surface will namely be closest to the actual one, as they are close to spherical shape. As the computation of SSA is based on the assumption of spheres, a shape factor larger than unity (i.e. $\xi > 1$) is necessary to correct for non-spherical shape, i.e. a positive displacement of all data points parallel to the axis of abscissa (increase of SSA). Hence, the material having the lowest slope (δ) could serve as model particle to calibrate the others. Finding the lowest slope for the materials with the most sphere-like shape could already serve as a simple validation of the presented approach.

In order to further validate the proposed relation between S_{sph} and E_p, shape factors have been selected in a next step. This selection was based on the work of [30] and is as a matter of fact not related to measured properties of the materials evaluated. In this way the different cement types were assigned with same shape factors of equivalent cement types from Reschke's research, e.g. a limestone powder was given the averaged shape factor for limestone powders taken from [30]. These selected shape factors are given in Table 6. It should be understood that they will only serve as a first comparison. However, plotting the newly derived and now shape-corrected SSA against E_p results in an improved coefficient of determination, which is shown in Fig. 12b. This applies both for the powder materials in common fineness (scatter plot area) and the two materials with the high fineness of about 28,000 and 45,000 cm^2/cm^3.

Based on these considerations a particle shape factor ξ was derived to correct all available and only sphere-based SSA in such a way that they fit on the regression line given by the particles that come closest to spherical shape (i.e. $\xi = 1$), which in this case is fly ash (cp. Fig. 12a). The equation based on the fly ash then reads as

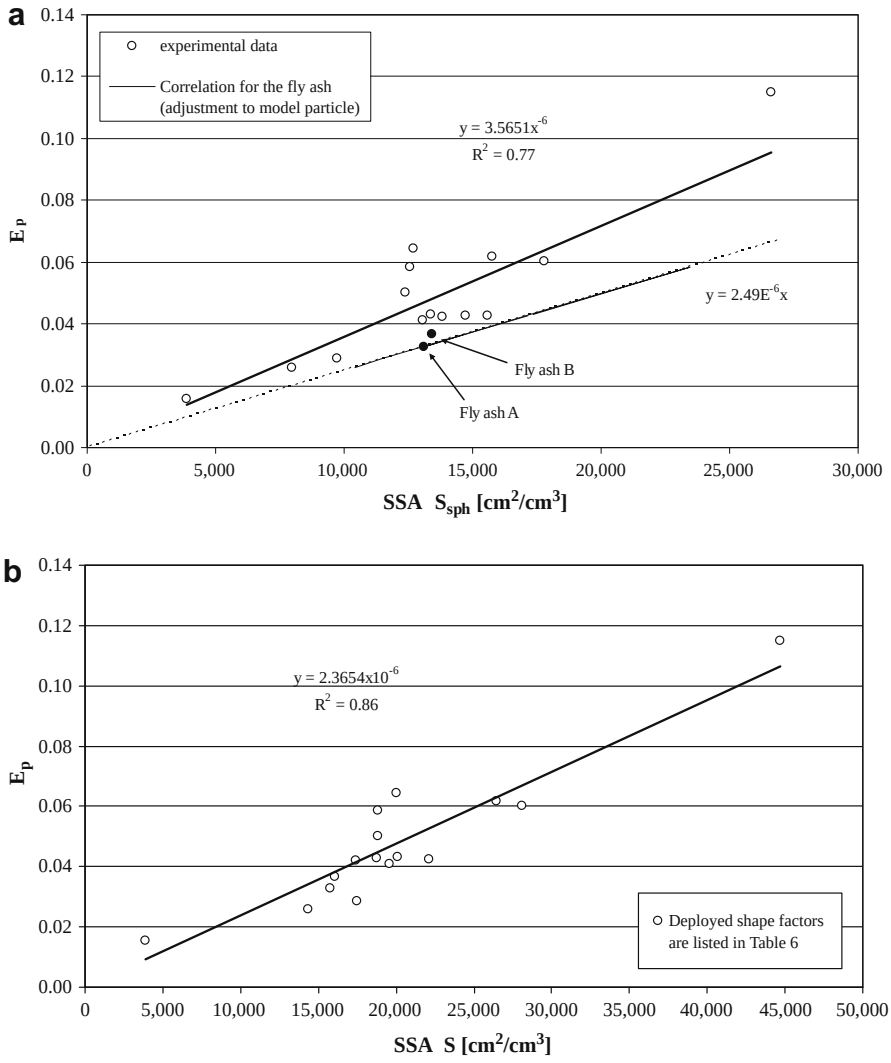

Fig. 12. (a) Plot of uncorrected, computed and volume based specific surface areas against the respective deformation coefficient E_p derived from spread-flow tests, showing the two involved fly ash materials. The dotted line represents the correlation of the fly ash, which is used for the derivation of the shape correction factor. (b) Plot of computed specific surface areas S and respective deformation coefficient. The SSA is now being corrected with shape factors based on [30].

Table 8
Volume based results on the spread-flow tests of the selected powder materials.

Material	Deformation coefficient E_p (–)	Parameter for water layer thickness, δ (cm)	Water demand, β_p (–)
Granite powder	0.0410	3.14×10^{-6}	1.2151
CEM III/B 42.5 N A	0.0643	5.07×10^{-6}	0.976
CEM III/B 42.5 N B	0.0603	3.39×10^{-6}	1.124
CEM I 52.5 R – micro-cement	0.1151	4.32×10^{-6}	1.730
Fly ash A[a]	0.0327	2.49×10^{-6}	0.524
Fly ash B	0.0366	2.73×10^{-6}	0.532
Limestone powder	0.0422	3.05×10^{-6}	0.754
Marble powder A	0.0426	2.89×10^{-6}	0.874
Marble powder B	0.0585	4.65×10^{-6}	1.005
Marble powder C	0.0432	3.23×10^{-6}	0.829
Gypsum A	0.0259	3.25×10^{-6}	0.673
Gypsum B	0.0287	2.95×10^{-6}	0.579
Trass flour	0.0428	2.74×10^{-6}	1.061

[a] The fly ash is used as calibration standard for the shape factor computation.

$$E_p = \delta \cdot a \cdot \rho_s = 2.49 \cdot 10^{-6} \cdot S \text{ with } \delta = 2.49 \cdot 10^{-6} \text{ cm} \quad (21)$$

Now, substituting E_p with the associated deformation coefficients determined by the spread-flow experiments and assuming a film thickness of 24.9 nm, for every material, a theoretical specific surface area S is computed. Comparing this theoretical surface with the uncorrected surface S_{sph}, which follows from Eq. (10) with ξ set equal to unity, a new shape correction factor ξ can be derived. This factor reads as

$$\xi = \frac{S}{S_{sph}} \quad (22)$$

Applying Eq. (22), shape factors have been computed for all given materials (cp. Table 6). It can be noticed that fitted shape factors correlate well with the ones based on [30] (cp. Fig. 13). This further validates the approach followed here. In total the shape factors range from 1.00 for the fly ash (as imposed here) up to 2.03 for the CEM III/B 42.5 N, the latter appearing to have the biggest shape deviation from smooth spheres. Note that all fitted shape factors are larger than unity indeed, which is consistent with the proposed approach. The second type of fly ash (fly ash B) yields a shape

factor only slightly higher than fly ash A. Differences in fly ash shape factors, also notably higher ones, can be explained by the partly porous surface structure, fly ash can possess. The surface structure of fly ash is highly dependent on the formation conditions. Furthermore, fly ash also can contain other types of ashes, unburnt coke particles, quartz particles or broken hollow balls. However, the assumed spherical shape, $\xi_{FA} = 1$, seems to be a good basis, as will also be seen in the next section. Furthermore, if fly ash would turn out to have a shape factor slightly larger than unity, all shape factors derived here only need to be multiplied with this $\xi_{FA} > 1$.

The authors are aware of the significant difference of the two slag cement shape factors. An explanation can be both, a change in the slag content as well as an error in the underlying PSD measurement.

4.2. SEM-image analysis

In order to further validate the derived shape factors and in particular to distinguish between particle geometry and surface roughness, SEM micrographs have been prepared and analyzed. Therefore, the preparation was executed by sprinkling small amounts of the dry powder on the sample carrier in order to achieve separated particles. In addition the sputtering process was repeated under varying angles to the vertical axis to assure full enveloping and connection to the conductive sample carrier. The SEM-images with a magnification factor of 1000 are exemplarily given in Fig. 14(a–f). Thereby the order of appearance from (a) to (f) corresponds to increasing shape factors as determined here (cp. Fig. 13). The glass beads (a) have not been introduced to the measurement yet since their monosized-like behavior causes problems during the spread-flow tests. However, their ideal spherical shape and the smooth surface justify an application as model particles for adjusting the shape factor derivation. Next, the fly ash A (b) is for the most part composed of spherical particles, but as described earlier, to some extent they show porous surfaces or contain other materials. The dolomitic marble powder A (c) is already notable less spherical but still providing a smooth surface, which explains the only slightly higher shape factor. A similar situation can be observed for the limestone powder (d) but here the surface appears to be rougher, resulting in a higher shape factor. The blast-furnace cement (e) shows highly angular shapes for the ground slag particles but having a smooth surface. Therefore, the shape factor still is comparable with for example the limestone powder. Finally, the micro-cement (f) shows angular particles with rough surface and therefore achieves the highest shape factor for this set of selected powders. This visual analysis strengthens the computational model and the shape factors derived here.

4.3. Concept of constant water layer thickness

From Eq. (21) a value of 24.9 nm was derived for δ of fly ash, representing a constant water layer thickness. Note that this model is based on the computed specific surface area and calibration using fly ash particles as spherical model particles, and is confirmed by the results of other powders. Although this layer thickness is in a similar range like the one derived by Brouwers and Radix [3] being 41.32 nm, there is still a difference of about 40%, which is analyzed in more detail here.

A most likely explanation is the difference of Blaine surface, used in [3], and computed surface used here. In the relevant literature most authors agree on linear correlation between Blaine fineness and the surface area calculated from PSD data. Robens [31] found, for instance, a constant factor of 1.3 for the ratio of computed surface area to Blaine. Applying this factor on the data presented here would increase the derived δ to 32.4 nm. For the readers interest it is noted, that this constant factor of 1.3, found by [31] is based on the automated surface computation of the deployed laser granulometer [32]. Its computation algorithm is based on a similar principle as described in Section 2 [14]. There the geometric mean of a class is considered as mean diameter, which results in larger surface areas compared to the arithmetic mean (cp. Eq. (8)). The difference between both surfaces amounts to about 6% considering a size ratio of $u = 2$ (as being used in standard sieve sets). Furthermore, the underlying model particles are spheres as well. Therefore the surface area difference of 1.3 is based on the assumption of spheres. Considering the true surface of the angular materials, which were actually cements in the example of [31], would make the deviation even bigger. Therefore, applying a shape factor in addition to the systematic deviation of Blaine surface and computed surface would result in an even increased water layer thickness. Depending on the shape factors selected, it is a range of 42–48 nm when deploying the derived shape factors for blast-furnace cements. This correlates with the film thicknesses found by [3] who used Blaine values, and by [16]. High correlation

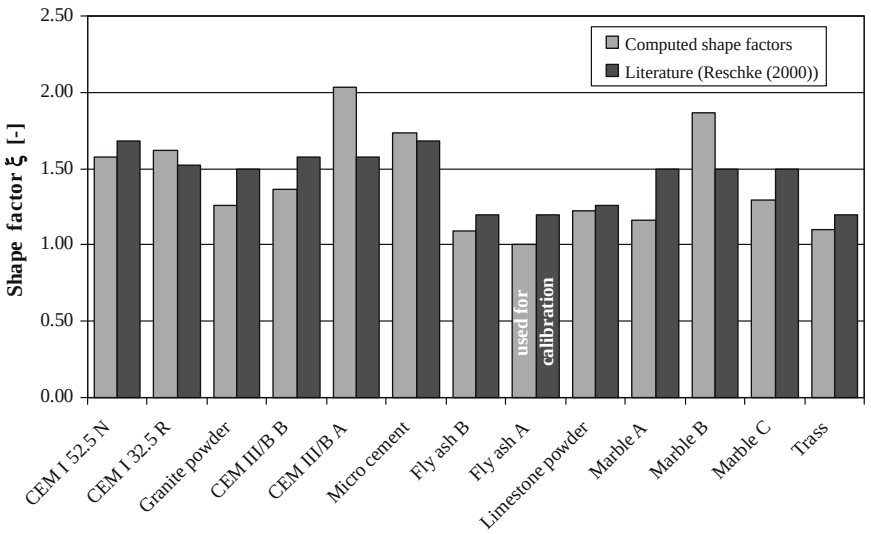

Fig. 13. Comparison of computed shape factors with the corresponding shape factors, selected from [30].

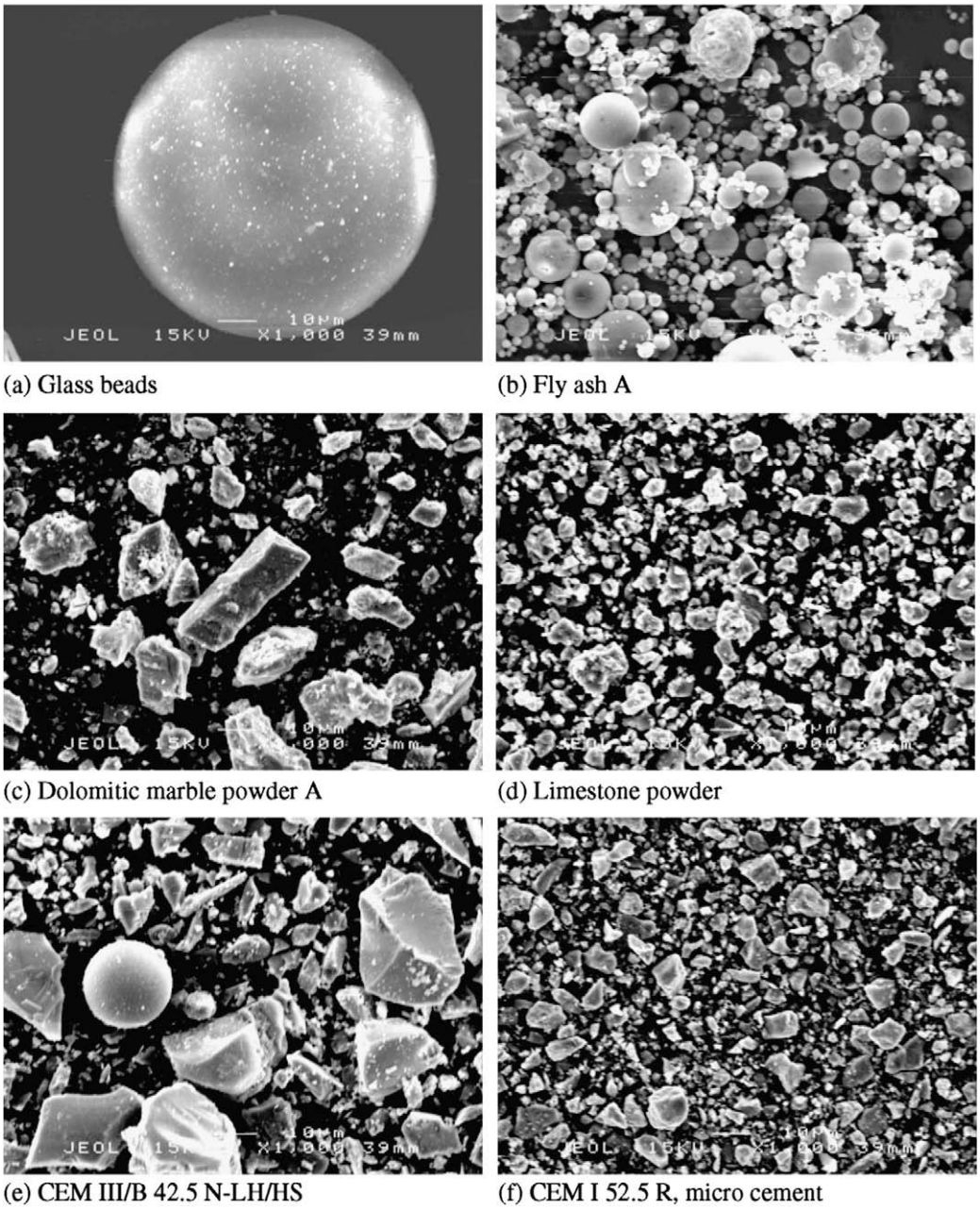

Fig. 14. SEM micrographs of the investigated powders, 1000-times magnified.

between computed surface area and Blaine fineness was also found by Hunt [13], who derived a factor of 0.97. However, the two correlation factors from [31] and [13] cannot directly be compared since the latter based the surface area computation on cumulative mass distribution curves derived by sedimentation method. Furthermore, the addressed specific surface area calculation method is based on the assumption of spheres and deploys the arithmetic mean of d_i and d_{i+1} as characteristic diameter (see Eq. (8)). A linear relation of computed specific surface area and measured Blaine surface is manifold confirmed in literature. Varying measurement techniques and different theoretical models, however, make their comparison difficult.

An analysis in this respect for the involved powders also results in a linear correlation, but with a higher factor indeed. For a number of powders the Blaine value was determined and multiplied with the respective specific density. These values have been plotted versus the computed SSA, now shape-corrected by the present model. By means of linear regression a correlation factor of 1.70 was found (cp. Fig. 15) via

$$S = 1.696 \cdot a_{\text{Blaine}} \cdot \rho_s \tag{23}$$

This increased ratio is explained by the shape correction, which now is included in this consideration. Taking the water layer thickness $\delta = 41.32$ nm from [3] again, which is based on Blaine, and using the derived factor between the surfaces, results in $\delta = 24.4$ nm as well. This should be understood as a correction of the systematic error of Blaine and the sphere assumption of the surface computation models. Hence, both derived water films, $\delta = 24.4$ nm following from [3] when Blaine surface is adjusted, as well as $\delta = 24.9$ nm with the presented study, are in close agreement with each other.

It should be noted that the coefficient of determination in Fig. 15 would turn to 0.91 when considering the marble powder

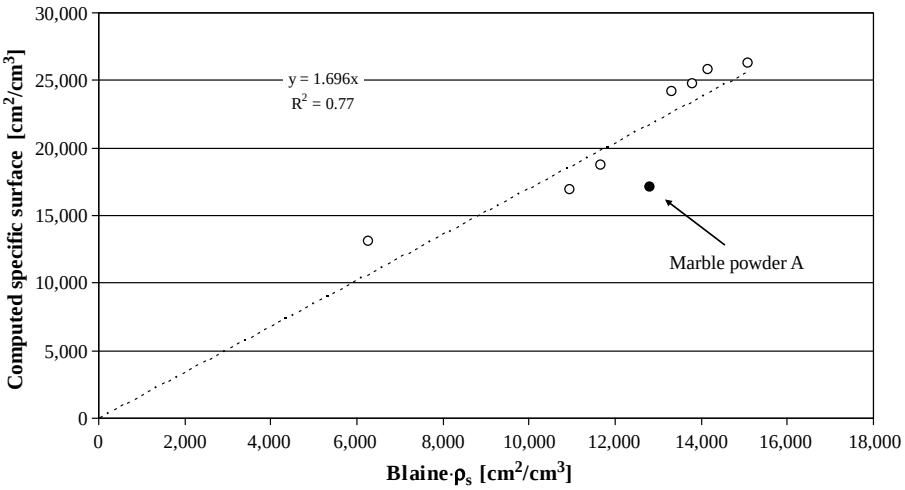

Fig. 15. Comparison of Blaine surface area and computed SSA. Both measures consider the true surface and are volume based, values are taken from Table 6.

as an outlier. Then the slope of the linear function changes from 1.70 to 1.75.

5. Conclusion

The present work first addresses the comparison of four different test methods for the determination of water demands of powders (i.e. particles < 125 μm), viz. spread-flow test, Puntke test, Vicat test and modified Marquardt test. Different correlations have been derived which express these values in terms of each other. Some of them are confirmed by literature, others are new. This applies for the recent, modified Marquardt test in comparison with the standard SCC spread-flow test.

1. A general trend between the several measurements was found in the order Puntke test, modified Marquardt method, Vicat test, and spread-flow experiments, from lowest to highest figures.
2. In general the modified Marquardt test was assessed to be a good technique for determining water contents. High precision of results even qualifies this technique for quality monitoring purposes of fineness or PSD changes of powder materials (in case no laser diffraction or similar technique is available).
3. The importance of the spread-flow test as one of the major test methods for SCC design is confirmed. New figures have been derived from it, which allow for the computation of water film thicknesses. Furthermore, the results show that the Puntke method and modified Marquardt method provide results in the same magnitude with Marquardt values being 1.04 times higher than Puntke values. Therefore, in the further course of the experiments, the Marquardt method was chosen since it has been the more precise method, resulting in reproducible measures, independent from an operator.
4. The spread-flow test will directly result in water demands being suitable for the design and production of self-compacting mixes. The modified Marquardt method is also expected to deliver information on the deformability of mixes. Since, similar to the spread-flow test, a granular mix is investigated in the state of flux, there should be equal information available. While having a free spread-flow of a water–powder mixture using the spread-flow test, for the addressed method the water–powder mixture is kept in motion by exposing it to a constant shear rate. Therefore, the change in power consumption should also give an indication on the sensitivity of the flow behavior to a certain dosage of water. This is understood as an equivalent to the deformation coefficient E_p of the spread-flow test.
5. Based on simple flow experiments, a shape factor can be derived, which is needed to correct a computed specific surface area, derived from PSD data. This approach is new and shows an interesting alternative to the existing, extensively device-related direct measurement principles. Besides the approach introduced by Reschke [30], this is to the author's knowledge the first technique using sound standard measurements for the derivation of a shape factor, which considers form, angularity and surface structure of powder materials. Furthermore, it gives new significance to the spread-flow test.
6. Different correlations of Blaine surface and computed SSA can be found in literature, and were proven by own experiments (Eq. (23)). Here a constant ratio of 1.70 (or 1.75) is found. Since the Blaine test is a simple and widely-used measurement, the derived correlation can be used to translate Blaine figures into computed figures based on PSDs (or backwards) which appears to result in information of equivalent or better accuracy. Furthermore, also fine particles, not being suitable for Blaine measurement can be expressed as "Blaine values".
7. In this article a water layer thickness of about 25 nm is found for flowing mixtures on the onset of flowing, i.e. having water contents of $V_w/V_p = \beta_p$. Hereby the derived water layer thickness is based on the computed specific surface area. This obtained value corresponds with the figure found by [3], when the differences in computed SSA and Blaine SSA are considered. The thickness amounts to about 40 nm when Blaine surface is considered. With the specific surface area and the corresponding water layer thickness, E_p can be predicted.
8. The hypothesis proposed by Brouwers and Radix [3] is confirmed. According to them the relative slump of a paste becomes a function of the SSA when sufficient water is present for flow.

The above findings are subject to further analysis and verification in order to find a place in a new concrete mix design concept, which is mainly based on particle size distribution, packing and specific surface area considerations and excess water. Also the hypothesis of constant water layers will be extended to mortars, and presents a new concept for the water demand of mortars and concrete in the framework of mix design.

References

[1] Powers TC. The properties of fresh concrete. New York: J. Wiley & Sons; 1968.
[2] Taylor HFW. Cement chemistry. 2nd ed. London: Thomas; 1997.
[3] Brouwers HJH, Radix HJ. Self-compacting concrete: theoretical and experimental study. Cem Concr Res 2005;35:2116–36 [Erratum, Cem Concr Res 2007;37:1376].
[4] Hunger M, Brouwers HJH. Natural stone waste powders applied to SCC mix design. Restor Build Monum 2008;14(2):131–40.
[5] Chen W. Hydration of slag cement – theory, modeling and application. PhD thesis. Enschede, University of Twente, The Netherlands; 2006.
[6] Calmon JL, Moratti M, Moraes S, Cenci D. Self-compacting concrete using marble and granite sawing wastes as filler. In: Proceedings 2005 World sustainable building conference, Tokyo; 2005. p. 4146–53.
[7] Laskaridis K. Personal contact. Laskaridis Marble S.A., Thassos, Greece; 2006.
[8] Ho DWS, Sheinn AMM, Ng CC, Tam CT. The use of quarry dust for SCC applications. Cem Concr Res 2002;32(4):505–11.
[9] McGeary RK. Mechanical packing of spherical particles. J Am Ceram Soc 1961;44(10):513–22.
[10] Onoda GY, Liniger EG. Random loose packings of uniform spheres and the dilatancy onset. Phys Rev Lett 1990;64(22):2727–30.
[11] Brunauer S, Emmett PH, Teller E. Adsorption of gases in multimolecular layers. J Am Chem Soc 1938;60(2):309–19.
[12] McCabe W, Smith JC. Unit operations of chemical engineering. New York: McGraw-Hill Book Company, Inc.; 1956.
[13] Hunt LP, Elspass CW. Particle-size properties of oilwell cements. Cem Concr Res 1986;16(6):805–12.
[14] Sympatec GmbH. Software algorithm for the derivation of the PSD-based specific surface area for WINDOX/HELOS-DOS 4.7. Germany: Clausthal-Zellerfeld; 2001.
[15] Ertingshausen H. Concrete made with sandrich particle fractions. Betonwerk + Fertigteiltechnik – BFT 1988;11:64–72.
[16] Marquardt I. Determination of the composition of self-compacting concretes on the basis of the water requirements of the constituent materials – presentation of a new mix concept. Betonwerk + Fertigteiltechnik – BFT 2002;11:22–30.
[17] Lambe TW. Soil stabilization. In: Leonards GE, editor. Foundation engineering. New York: McGraw-Hill; 1962.
[18] Stumm W. Chemistry of the solid-water interface – processes at the mineral–water and particle–water interface in natural systems. New York: John Wiley & Sons Inc.; 1992.
[19] Okamura H, Ozawa K. Mix-design for self-compacting concrete. Concre Lib, JSCE 1995;25:107–20.
[20] Domone PL, HsiWen C. Testing of binders for high performance concrete. Cem Concr Res 1997;27(8):1141–7.
[21] DAfStb – Deutscher Ausschuss für Stahlbeton. Richtlinie "Selbstverdichtender Beton" (SVB-Richtlinie), 'SCC directive' 2001. Berlin: Beuth Verlag GmbH; 2001.
[22] Okamura H, Ouchi M. Self-compacting concrete. J Adv Concr Tech Jpn Concr Inst 2003;1(1):5–15.
[23] Puntke W. Wasseranspruch von feinen kornhaufwerken. Beton 2002;5:242–8 [in German].
[24] Amziane S. Setting time determination of cementitious materials based on measurements of the hydraulic pressure variations. Cem Concr Res 2006;36(2):295–304.
[25] Lichtmann M, Bottke R. Concrete testing method and apparatus suitable for use with both low and high water content concrete for determining density, air content and, after hardening in the mold, tensile strength. DE-patent DE10008664; 2001.
[26] Lichtmann M, Groß A. Practice related determination of the optimal water content. Betonwerk + Fertigteiltechnik – BFT 2003;6:6–14.
[27] Bornemann R. Untersuchung zur Modellierung des Frisch-und Festbetonverhaltens erdfeuchter Betone. Ph.D. thesis, Kassel, University of Kassel; 2005 [in German].
[28] Fung WWS, Kwan AKH, Wong HHC. Wet packing of crushed rock fine aggregate. Mater Struct, accepted for publication, doi: 10.1617/s11527-008-9409-3.
[29] Marquardt I. Ermittlung des wasseranspruchs von feinteiligen ausgangsstoffen für Beton. Beton. 2003;10:490–2 [in German].
[30] Reschke T. Der Einfluß der Granulometrie der Feinstoffe auf die Gefügeentwicklung und die Festigkeit von Beton. Ph.D. thesis, Weimar, Bauhaus Universität Weimar; 2000 [in German].
[31] Robens E, Benzler B, Büchel G, Reichert H, Schumacher K. Investigation of characterizing methods for the microstructure of cement. Cem Concr Res 2002;32(1):87–90.
[32] Robens E. Personal contact; 2007.